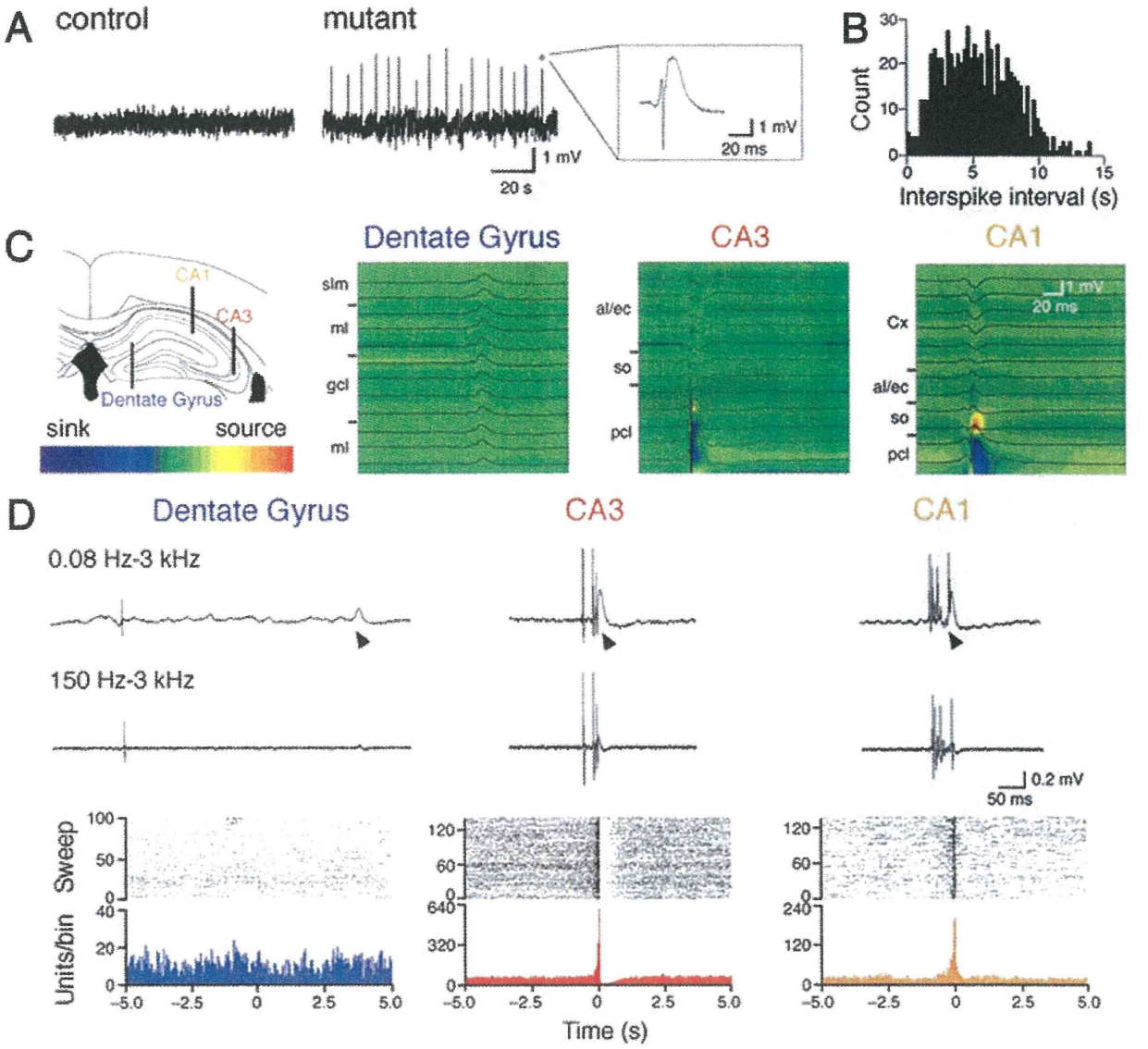

Figure 6. Characteristic large EEG spikes in the hippocampal CA3 region of mutant mice. **A**, Representative local field potential recordings from the CA3 region. **B**, Histogram of interspike intervals (bin, 0.25 s). **C**, Laminar profiles of field potentials and CSD analysis. Recording positions are illustrated on the left. Sinks and sources are indicated by cold and warm colors, respectively. Abbreviations: al/ec, alveus and external capsule; Cx, cortex; gcl, granule cell layer; ml, molecular layer; pcl, pyramidal cell layer; slm, stratum lacunosum-moleculare; so, stratum oriens. **D**, Wide-band recordings of extracellular activities (top), filtered MUA (middle) and raster plots and peri-event time histograms between MUA (bin, 200 ms) and EEG spikes in the dentate gyrus (left), CA3 (center) and CA1 regions (right). Arrowheads indicate the onset of spikes. MUA were aligned to the onset of spikes (time 0).
doi:10.1371/journal.pone.0003993.g006

(control, 0.52 ± 0.09; mutant, 0.61 ± 0.16; $n=12$ each; t-test, $P=0.65$) (Fig. 7B). Thus, there was no significant electrophysiological imbalance between AMPA receptor-mediated excitatory and $GABA_A$ receptor-mediated inhibitory synaptic transmission in the hippocampal CA3 region.

High-frequency stimulation failed to induce slow hyperpolarizing currents in hippocampal CA3 pyramidal neurons of mutant mice

In hippocampal CA1 pyramidal neurons, synaptic excitation is followed by an early GABA-mediated hyperpolarization and late AHP mediated by Ca^{2+}-dependent K^+ channels [40]. We thus examined the effect of NMDA receptor ablation on Ca^{2+}-dependent K^+ channels in hippocampal CA3 neurons. At a holding potential of -20 mV, high-frequency stimulation, which should activate both AMPA receptors and NMDA receptors in normal mice, induced slowly decaying outward currents in the pyramidal cells of control mice (Fig. 7C; peak amplitude, 46.1 ± 5.4 pA, $n=12$). In contrast, such slow outward currents were hardly evoked by the same high-frequency stimulation in mutant mice (Fig. 7C; 0.5 ± 2.1 pA, $n=12$, $P<0.001$). The outward currents in control mice were abolished by D-APV (Fig. 7D; control, 46.13 ± 5.36 pA, $n=13$; D-APV, 0.38 ± 2.41 pA, $n=12$,

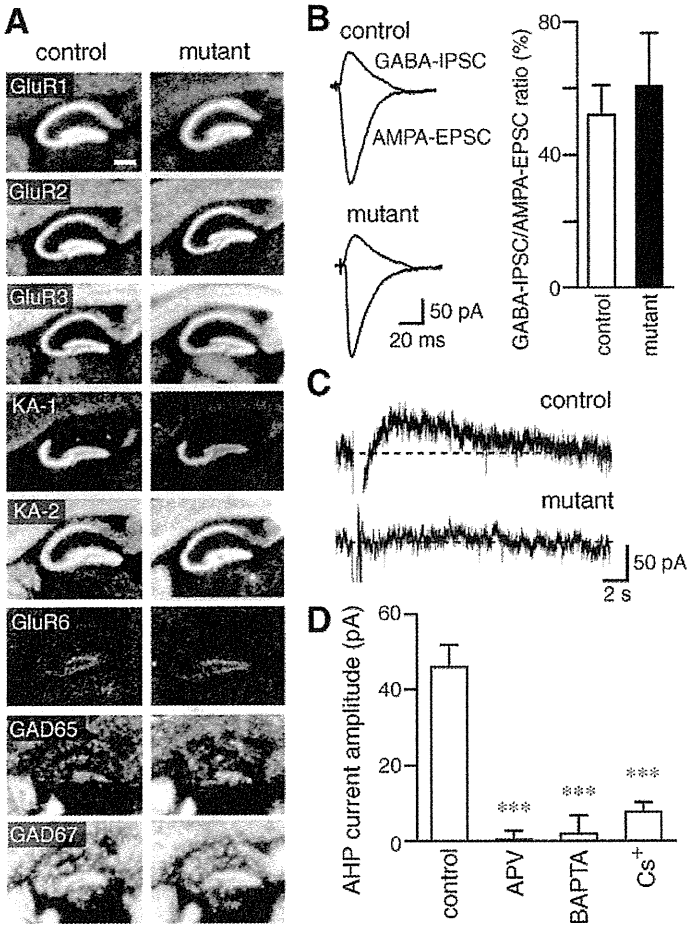

Figure 7. High-frequency stimulation failed to induce slow hyperpolarizing currents in hippocampal CA3 pyramidal neurons of mutant mice. A, X-ray film autoradiography for mRNAs of AMPA receptors, kainate receptors, and GADs. Scale bar, 200 μm. **B**, Representative traces of AMPA-EPSCs and $GABA_A$-IPSCs in the CA3 pyramidal cells. Graph shows the ratio of $GABA_A$-IPSCs to AMPA-EPSCs. **C**, Representative traces of slow hyperpolarizing currents. **D**, Peak amplitudes of the slow hyperpolarizing currents of the control mice in the absence (control) or presence of D-APV. Those recorded with a BAPTA-containing (BAPTA) or Cs^+-based internal solution (Cs^+) are also shown. ***, P<0.001, *t*-test.
doi:10.1371/journal.pone.0003993.g007

Table 1. Ratios of hybridization signal densities of GluR and GAD mRNAs in the CA3 region to those in the CA1 region.

mRNA	Control	Mutant
GluRζ1/NR1	0.86±0.02 (*n*=10)	0.04±0.01 (*n*=5)
GluRα1/GluR1	0.98±0.02 (*n*=10)	0.95±0.01 (*n*=12)
GluRα2/GluR2	0.91±0.03 (*n*=8)	0.89±0.03 (*n*=11)
GluRα3/GluR3	0.88±0.02 (*n*=10)	0.86±0.02 (*n*=12)
GluRγ2/KA-2	1.16±0.03 (*n*=9)	1.17±0.02 (*n*=10)
GluRβ2/GluR6	1.11±0.09 (*n*=8)	1.19±0.04 (*n*=8)
GAD65	1.12±0.05 (*n*=10)	0.99±0.05 (*n*=11)
GAD67	1.11±0.02 (*n*=10)	0.94±0.03 (*n*=12)

Slices were prepared from 3 mice of both genotypes.
Hybridization signal densities of the *GluRγ1/KA-1* mRNA in the CA3 region were 51.5±0.8 (*n*=10) in control mice and 32.3±0.5 (*n*=12) in mutant mice.
doi:10.1371/journal.pone.0003993.t001

P<0.001), suggesting that NMDA receptors are required for the response. NMDA receptor activation results in influx of Ca^{2+} into postsynaptic cells, which would activate Ca^{2+}-dependent K^+ channels. In fact, inclusion of the Ca^{2+} chelator BAPTA in the internal solution of patch pipettes diminished the outward currents (Fig. 7D; BAPTA, 1.99±4.76 pA, $n=7$, $P<0.001$). The outward currents were also diminished when recorded with a Cs^+-based internal solution (Fig. 7D; Cs^+, 7.74±2.35 pA, $n=4$, $P<0.001$), suggesting that the currents were mediated by postsynaptic K^+ channels. Taken together, the slow kinetics and sensitivities to D-APV, BAPTA and Cs^+ of the outward hyperpolarizing currents suggest that the high-frequency stimulation evokes slow AHP currents [41,42] mediated by Ca^{2+}-activated K^+ channels, which are activated by Ca^{2+} influx through NMDA receptor channels. These results suggest that the NMDA receptor-slow AHP coupling is diminished in the hippocampal CA3 pyramidal neurons of mutant mice, which may result in enhanced excitability of the CA3 recurrent network as a whole. The coupling between NMDA receptors and AHP currents is found in various regions [34,43–45]. However, the durations of AHP currents observed in our

experiment were much longer than those observed in previous studies.

These results with hippocampal CA3-specific NMDA receptor mutant mice raise an intriguing possibility that MDA receptors suppress the excitability of the CA3 recurrent network as a whole by restricting synchronous firing of CA3 neurons, although the possibility cannot be excluded that the enhanced excitability of the mutant mice might be due to subtle cytoarchitectural abnormalities of CA3 pyramidal neurons. To test the possibility, we then examined the effect of NMDA receptor ablation in the CA3 region of the adult brain on hippocampal network oscillations by employing a virus-mediated gene knockout technique [22,23].

Ablation of CA3 NMDA receptors in the mature brain also generated characteristic EEG spikes with large amplitudes

An adeno-associated viral expression vector for Cre recombinase (AAV-Cre, titer of $5–8\times10^{10}$) was streotaxically microinjected to the hippocampal CA3 region of *GluRζ1*$^{flox/flox}$ mice at 8–9 weeks old. Immunohistochemical analysis revealed that the infection of AAV-Cre was limited to the hippocampal CA3 region and spread within 40–70% of the region (Fig. 8A–C). Immunoreactivity for GluRζ1 was diminished in the well-demarcated infected CA3 region by 2 weeks after infection (Fig. 8C). Age-matched *GluRζ1*$^{+/+}$ mice microinjected with AAV-Cre served as controls.

Local field potential recording from the CA3 region showed characteristic EEG spikes with large amplitudes in *GluRζ1*$^{flox/flox}$ mice 2–3 weeks after AAV-Cre infection ($n=5$ out of 9 mice) (Fig. 8D). The frequency of large EEG spikes was variable among subjects, which may be related to the variance of AAV-infected regions among animals. No such spike activity was detected in EEG records from the CA3 region of AAV-Cre-infected *GluRζ1*$^{+/+}$ mice ($n=7$ out of 7 mice, $P=0.02$, Fisher's exact probability test) (Fig. 8D). CSD analysis revealed the sink in the pyramidal cell layer of the CA3 region and the sources in neighboring stratum oriens (Fig. 8E, $n=8$ spikes). Thus, the ablation of CA3 NMDA receptors induced by AAV-Cre infection in the adult brain also resulted in the generation of characteristic EEG spikes.

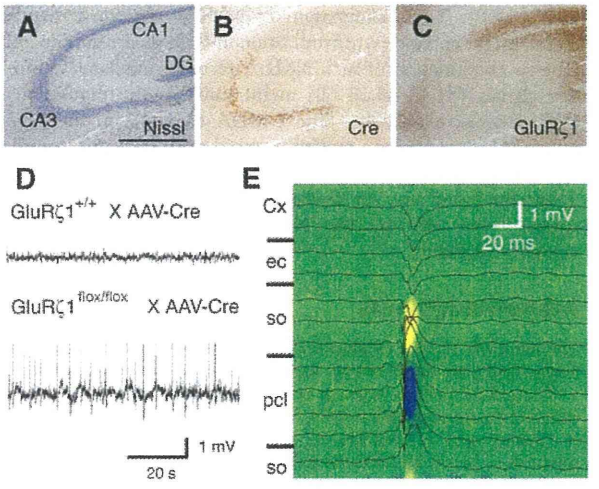

Figure 8. Hippocampal CA3 NMDA receptor ablation in the adult brain also generated characteristic EEG spikes with large amplitudes. A–C, AAV-Cre-mediated ablation of NMDA receptors in the hippocampal CA3 region. Nissl staining (**A**) and imunohistochemistry for Cre (**B**) and GluRζ1 (**C**). Scale bar, 0.5 mm. **D**, Representative local field potential recordings from the CA3 region. **E**, Laminar profiles of field potentials and CSD analysis. Recording positions are illustrated on the left. Sinks and sources are indicated by cold and warm colors, respectively. Cx, cortex; ec, external capsule; pcl, pyramidal cell layer; so, stratum oriens.
doi:10.1371/journal.pone.0003993.g008

Pharmacological blockade of CA3 NMDA receptors enhanced the susceptibility to kainate-induced seizure

We finally examined the seizure susceptibility of wild-type mice by focal injection of a competitive NMDA receptor antagonist, APV. We bilaterally injected 30 mM APV or aCSF into the hippocampal CA3 region of C57BL/6N mice at postnatal 8–10 weeks. About 20–30 minutes later, the animals were intraperitoneally administrated with the convulsive dose of kainate (30 mg/kg) [46]. Kainate-induced tonic-clonic seizures with loss of the postural tone appeared within 1 h in both groups of mice ($n=8$ each; $P=0.23$, Fisher's exact probability test) (Fig. 9). However, the latency to the onset of seizures was significantly shorter in mice injected with APV ($n=8$; $P=0.0044$, Log-rank test). Thus, the focal blockage of CA3 NMDA receptors also enhanced the susceptibility to kainate-induced seizure.

Discussion

Here, we generated hippocampal CA3 pyramidal neuron-specific NMDA receptor mutant mice on the C57BL/6N genetic background. The expression of the *GluRζ1* mRNA was comparable between mutant and control mice at P1 but strongly decreased in mutant mice at P7. The significant expression of GluRζ1 protein, though reduced, was found in the CA3 region at P7 but diminished to a negligible level by P14. We found that the mutant mice lacking NMDA receptors in the hippocampal CA3 pyramidal neurons showed enhanced susceptibility to kainate-induced seizures. This observation was rather unexpected since NMDA receptor-mediated LTP was implied to contribute to the generation of synchronous network activity by *in vitro* studies [14,15]. We found that characteristic EEG spikes with large amplitude were generated by the ablation of NMDA receptors in CA3 pyramidal neurons. Strong association of MUA with the characteristic EEG spikes in the CA3 pyramidal cell layer of mutant mice suggests that the CA3 NMDA receptor ablation increases the synchronous network activity possibly by affecting the firing pattern of CA3 neurons. In contrast, CA1 region-specific ablation of NMDA receptors appeared to hardly affect EEG *in vivo* [47]. NMDA receptor antagonists have minimal effects on basal synaptic transmission but completely block the generation of long-term potentiation in the CA1 region *in vitro* [48–50]. Hence, NMDA receptors in the CA1 region are not considered to be involved in spontaneous network activity. The difference in the neural wiring pattern such as the abundance of recurrent networks may underlie the different effects of NMDA receptor ablation in the hippocampal CA1 and CA3 regions on network activity. Our results raise an intriguing possibility that NMDA receptors may suppress the excitability of the CA3 network as a whole *in vivo*.

It is possible that the ablation of NMDA receptors may disturb the neural wiring of the hippocampal CA3 region, leading to abnormal excitability of the network. It is well known that the NMDA receptor plays a role in the activity-dependent refinement of synaptic connections and neural pattern formation [51–54]. Chronic blockade of NMDA receptors in hippocampal slice cultures during the first two weeks of postnatal development leads to a substantial increase in synapse number and results in a more complex dendritic arborization of CA1 pyramidal cells [31]. The activity blockade in hippocampus during postnatal 2–3 weeks by

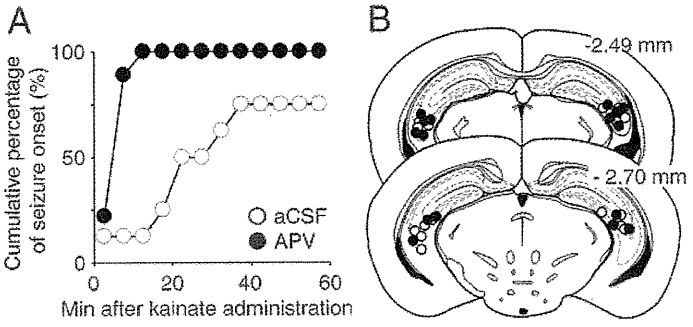

Figure 9. The pharmacological blockade of CA3 NMDA receptors increased the susceptibility to kainate-induced seizures. A, Cumulative curves for the onset of seizure. **B,** Illustration of the injection sites of APV (filled) and aCSF (open). Numbers represent distance (mm) of the section relative to the bregma landmark.
doi:10.1371/journal.pone.0003993.g009

tetrodotoxin infusion produced both behavioral and electrographic seizures 2 weeks after the infusion [55] and the increase in the density of axonal varicosities and postsynaptic AMPA receptor GluR1 and NMDA receptors [56]. Thus, reduced neuronal activity during development might potentially enhance the excitability. However, the cytoarchitecture was indistinguishable between control and mutant mice at P21–23. There were no detectable differences in the dendritic branching and the density of axonal boutons and dendritic spines between control and mutant mice at P21–23. The sustained expression of NMDA receptor proteins at least by P7 in mutant mice may support the development of CA3 pyramidal neuron cytoarchitectures. An alternative possibility is that the excitability of the CA3 network may be suppressed by NMDA receptor-mediated signaling. No significant differences were detectable in the basic membrane properties and balance between excitatory and inhibitory synaptic transmission between control and mutant mice. At synapses, activation of NMDA receptors evokes excitatory postsynaptic potential on the CA3 pyramidal neurons *in vitro* [57]. However, the enhancement of the kainate-induced seizure susceptibility and the emergence of characteristic EEG spikes associated with MUA in the mutant mice can be hardly explained if major roles of NMDA receptors would be simply mediating and strengthening the excitatory transmission at the commissural/associational synapses. Besides excitatory transmission and its enhancement, NMDA receptors may mediate diverse suppressive signals including spike-timing dependent long-term depression [58], LTP of slow GABA-IPSCs [59], the increase in I_h currents [60], and coupling with K^+ channels [34,43–45]. Thus, it is possible that NMDA receptor signaling may suppress the excitability of the CA3 network *in vivo*, although the possibility cannot be excluded that the enhanced excitability of the mutant mice might be due to subtle developmental abnormalities of CA3 pyramidal neurons.

We thus examined whether the excitability of the CA3 network is enhanced by ablation of NMDA receptors in the adult brain with a virus-mediated gene knockout technique [22,23]. We found that EEG spikes with large amplitude were generated by focal ablation of NMDA receptors in the CA3 region of adult mice by AAV-Cre infection. The frequency of large EEG spikes was variable among subjects, which may be related to the variance of AAV-infected regions among animals. Furthermore, the blockade of NMDA receptors by focal injection of APV into the hippocampal CA3 region enhanced the susceptibility to kainate-induced seizures. These results suggest that NMDA receptors control negatively the excitability of the hippocampal CA3 recurrent network as a whole *in vivo* by restricting synchronous firing of CA3 neurons, although the mechanism remains to be solved. Since slow AHP currents are involved in accommodation of action potential discharge of CA1 pyramidal neurons [40], it is possible that the frequency of action potentials may increase in a mutant CA3 pyramidal neuron where NMDA receptor-AHP coupling is eliminated. Prolonged discharges of CA3 pyramidal neurons might increase the chance of their synchronous firing, leading to the enhancement of the excitability of the CA3 network as a whole. Interestingly, Colgin et al. reported that blockade of NMDA receptors enhanced spontaneous sharp waves in rat hippocampal slices [61], supporting the idea that activation of NMDA receptors can serve to dampen the excitation of sharp waves. On the other hand, studies through computational models showed that when recurrent networks with conductance delays exhibit population bursts, spike-timing-dependent plasticity (STDP) rules exert a strong decoupling force that desynchronizes activity [58]. Thus, elimination of NMDA receptor-dependent STDP might enhance synchronization in CA3 recurrent networks. One or combination of such NMDA receptor-mediated suppressive signals [34,43–45,58–60] might underlie the regulation of CA3 network excitability. The NMDA receptors in the hippocampal CA3 region are implied in rapid acquisition and recall of associative memory as well as paired associate learning [11–13]. These functions may be mediated not only by the plasticity at synapses but also by the NMDA receptor-mediated neural network oscillation.

Acknowledgments

We thank Dr. H. Kashiwadani and Dr. K. Mori for valuable advice and help in field potential recordings and critical reading of the manuscript, Dr. Y. Kiyama for help in targeting vector construction, Ms R. Natsume for chimeric mouse preparation, Ms E. Kato for advice on Golgi staining, Mrs N. Takino and H. Nishida for technical assistance in AAV vector production, Ms A. Kishioka for help in animal surgery, Dr. T. Takeuchi for help in ES cell preparation, and Mrs H. Wakamatsu, Y. Takushi and T. Kurokawa for help in mice breeding. We are grateful to Dr. M. Ohtsuka for his encouragement and support. Thanks are also to Drs H. Iwama, I. Ito, Y. Takahashi and T. Tsujimoto for advice.

Author Contributions

Conceived and designed the experiments: FF KN MW TM MM. Performed the experiments: FF KN TS MF MW. Analyzed the data: FF KN TS MF MW. Contributed reagents/materials/analysis tools: SiM KS HK HM. Wrote the paper: FF KN MW TM MM.

References

1. Amaral DG, Witter MP (1989) The three-dimensional organization of the hippocampal formation: a review of anatomical data. Neuroscience 31: 571–591.
2. MacVicar BA, Dudek FE (1980) Local synaptic circuits in rat hippocampus: interactions between pyramidal cells. Brain Res 184: 220–223.
3. Miles R, Wong RK (1983) Single neurones can initiate synchronized population discharge in the hippocampus. Nature 306: 371–373.
4. Traub RD, Miles R (1991) Collective behaviours of the CA3 network: experiment and model. Neuronal Networks of The Hippocampus. Cambridge: Cambridge University Press. pp 119–156.
5. Buzsáki G (1989) Two-stage model of memory trace formation: a role for "noisy" brain states. Neuroscience 31: 551–570.
6. Jefferys JGR (1993) The pathophysiology of epilepsies. In: Laidlaw J, Richens A, Chadwick D, eds. A Textbook of epilepsy. 4th ed. Edinburgh: Churchill Livingstone. pp 241–276.
7. Csicsvari J, Hirase H, Czurko A, Buzsáki G (1998) Reliability and state dependence of pyramidal cell-interneuron synapses in the hippocampus: an ensemble approach in the behaving rat. Neuron 21: 179–189.
8. Ylinen A, Bragin A, Nádasdy Z, Jandó G, Szabó I, et al. (1995) Sharp wave-associated high-frequency oscillation (200 Hz) in the intact hippocampus: network and intracellular mechanisms. J Neurosci 15: 30–46.
9. Morris RG (2003) Long-term potentiation and memory. Philos Trans R Soc Lond B Biol Sci 358: 643–647.
10. Jonas P, Major G, Sakmann B (1993) Quantal components of unitary EPSCs at the mossy fibre synapse on CA3 pyramidal cells of rat hippocampus. J Physiol 472: 615–663.
11. Nakazawa K, Quirk MC, Chitwood RA, Watanabe M, Yeckel MF, et al. (2002) Requirement for hippocampal CA3 NMDA receptors in associative memory recall. Science 297: 211–218.
12. Nakazawa K, Sun LD, Quirk MC, Rondi-Reig L, Wilson MA, et al. (2003) Hippocampal CA3 NMDA receptors are crucial for memory acquisition of one-time experience. Neuron 38: 305–315.
13. Rajji T, Chapman D, Eichenbaum H, Greene R (2006) The role of CA3 hippocampal NMDA receptors in paired associate learning. J Neurosci 26: 908–915.
14. Bains JS, Longacher JM, Staley KJ (1999) Reciprocal interactions between CA3 network activity and strength of recurrent collateral synapses. Nat Neurosci 2: 720–726.
15. Behrens CJ, van den Boom LP, de Hoz L, Friedman A, Heinemann U (2005) Induction of sharp wave-ripple complexes in vitro and reorganization of hippocampal networks. Nat Neurosci 8: 1560–1567.
16. Yamazaki M, Mori H, Araki K, Mori KJ, Mishina M (1992) Cloning, expression and modulation of a mouse NMDA receptor subunit. FEBS Lett 300: 39–45.
17. Taniguchi M, Yuasa S, Fujisawa H, Naruse I, Saga S, et al. (1997) Disruption of semaphorin III/D gene causes severe abnormality in peripheral nerve projection. Neuron 19: 519–530.
18. Takeuchi T, Miyazaki T, Watanabe M, Mori H, Sakimura K, et al. (2005) Control of synaptic connection by glutamate receptor δ2 in the adult cerebellum. J Neurosci 25: 2146–2156.
19. Mishina M, Sakimura K (2007) Conditional gene targeting on the pure C57BL/6 genetic background. Neurosci Res 58: 105–112.
20. Takeuchi T, Nomura T, Tsujita M, Suzuki M, Fuse T, et al. (2002) Flp recombinase transgenic mice of C57BL/6 strain for conditional gene targeting. Biochem Biophys Res Commun 293: 953–957.
21. Werner P, Voigt M, Keinanen K, Wisden W, Seeburg PH (1991) Cloning of a putative high-affinity kainate receptor expressed predominantly in hippocampal CA3 cells. Nature 351: 742–744.
22. Li XG, Okada T, Kodera M, Nara Y, Takino N, et al. (2006) Viral-mediated temporally controlled dopamine production in a rat model of Parkinson disease. Mol Ther 13: 160–166.
23. Scammell TE, Arrigoni E, Thompson MA, Ronan PJ, Saper CB, et al. (2003) Focal deletion of the adenosine A1 receptor in adult mice using an adeno-associated viral vector. J Neurosci 23: 5762–5770.
24. Fukaya M, Kato A, Lovett C, Tonegawa S, Watanabe M (2003) Retention of NMDA receptor NR2 subunits in the lumen of endoplasmic reticulum in targeted NR1 knockout mice. Proc Natl Acad Sci U S A 100: 4855–4860.
25. Miyazaki T, Fukaya M, Shimizu H, Watanabe M (2003) Subtype switching of vesicular glutamate transporters at parallel fibre-Purkinje cell synapses in developing mouse cerebellum. Eur J Neurosci 17: 2563–2572.
26. Nakagawa S, Watanabe M, Isobe T, Kondo H, Inoue Y (1998) Cytological compartmentalization in the staggerer cerebellum, as revealed by calbindin immunohistochemistry for Purkinje cells. J Comp Neurol 395: 112–120.
27. Fukaya M, Watanabe M (2000) Improved immunohistochemical detection of postsynaptically located PSD-95/SAP90 protein family by protease section pretreatment: a study in the adult mouse brain. J Comp Neurol 426: 572–586.
28. Shimuta M, Yoshikawa M, Fukaya M, Watanabe M, Takeshima H, et al. (2001) Postsynaptic modulation of AMPA receptor-mediated synaptic responses and LTP by the type 3 ryanodine receptor. Mol Cell Neurosci 17: 921–930.
29. Yamada K, Fukaya M, Shimizu H, Sakimura K, Watanabe M (2001) NMDA receptor subunits GluRε1, GluRε3 and GluRζ1 are enriched at the mossy fibre-granule cell synapse in the adult mouse cerebellum. Eur J Neurosci 13: 2025–2036.
30. Watanabe M, Fukaya M, Sakimura K, Manabe T, Mishina M, et al. (1998) Selective scarcity of NMDA receptor channel subunits in the stratum lucidum (mossy fibre-recipient layer) of the mouse hippocampal CA3 subfield. Eur J Neurosci 10: 478–487.
31. Luthi A, Schwyzer L, Mateos JM, Gahwiler BH, McKinney RA (2001) NMDA receptor activation limits the number of synaptic connections during hippocampal development. Nat Neurosci 4: 1102–1107.
32. Fukaya M, Yamazaki M, Sakimura K, Watanabe M (2005) Spatial diversity in gene expression for VDCCγ subunit family in developing and adult mouse brains. Neurosci Res 53: 376–383.
33. Yamada K, Fukaya M, Shibata T, Kurihara H, Tanaka K, et al. (2000) Dynamic transformation of Bergmann glial fibers proceeds in correlation with dendritic outgrowth and synapse formation of cerebellar Purkinje cells. J Comp Neurol 418: 106–120.
34. Isaacson JS, Murphy GJ (2001) Glutamate-mediated extrasynaptic inhibition: direct coupling of NMDA receptors to Ca^{2+}-activated K^+ channels. Neuron 31: 1027–1034.
35. Murakami M, Kashiwadani H, Kirino Y, Mori K (2005) State-dependent sensory gating in olfactory cortex. Neuron 46: 285–296.
36. Franklin KBJ, Paxinos G (1996) The mouse brain in stereotaxic coordinates. San Diego: Academic Press.
37. Ben-Ari Y (1985) Limbic seizure and brain damage produced by kainic acid: mechanisms and relevance to human temporal lobe epilepsy. Neuroscience 14: 375–403.
38. Westbrook GL (2000) Seizures and Epilepsy. In: Kandel ER, Schwartz JH, Jessell TM, eds. Principles of Neural Science. 4th ed. Cambridge: Cambridge Univ Press. pp 910–935.
39. Lawrence JJ, McBain CJ (2003) Interneuron diversity series: containing the detonation—feedforward inhibition in the CA3 hippocampus. Trends Neurosci 26: 631–640.
40. Nicoll RA, Alger BE (1981) Synaptic excitation may activate a calcium-dependent potassium conductance in hippocampal pyramidal cells. Science 212: 957–959.
41. Schwartzkroin PA, Stafstrom CE (1980) Effects of EGTA on the calcium-activated afterhyperpolarization in hippocampal CA3 pyramidal cells. Science 210: 1125–1126.
42. Stocker M, Krause M, Pedarzani P (1999) An apamin-sensitive Ca^{2+}-activated K^+ current in hippocampal pyramidal neurons. Proc Natl Acad Sci U S A 96: 4662–4667.
43. Faber ES, Delaney AJ, Sah P (2005) SK channels regulate excitatory synaptic transmission and plasticity in the lateral amygdala. Nat Neurosci 8: 635–641.
44. Lin MT, Lujan R, Watanabe M, Adelman JP, Maylie J (2008) SK2 channel plasticity contributes to LTP at Schaffer collateral-CA1 synapses. Nat Neurosci 11: 170–177.
45. Ngo-Anh TJ, Bloodgood BL, Lin M, Sabatini BL, Maylie J, et al. (2005) SK channels and NMDA receptors form a Ca^{2+}-mediated feedback loop in dendritic spines. Nat Neurosci 8: 642–649.
46. Mulle C, Sailer A, Pérez-Otaño I, Dickinson-Anson H, Castillo PE, et al. (1998) Altered synaptic physiology and reduced susceptibility to kainate-induced seizures in GluR6-deficient mice. Nature 392: 601–605.
47. McHugh TJ, Blum KI, Tsien JZ, Tonegawa S, Wilson MA (1996) Impaired hippocampal representation of space in CA1-specific NMDAR1 knockout mice. Cell 87: 1339–1349.
48. Bear MF, Malenka RC (1994) Synaptic plasticity: LTP and LTD. Curr Opin Neurobiol 4: 389–399.
49. Bliss TV, Collingridge GL (1993) A synaptic model of memory: long-term potentiation in the hippocampus. Nature 361: 31–39.
50. Malenka RC, Nicoll RA (1999) Long-term potentiation—a decade of progress? Science 285: 1870–1874.
51. Cline HT, Debski EA, Constantine-Paton M (1987) *N*-methyl-D-aspartate receptor antagonist desegregates eye-specific stripes. Proc Natl Acad Sci U S A 84: 4342–4345.
52. Kleinschmidt A, Bear MF, Singer W (1987) Blockade of "NMDA" receptors disrupts experience-dependent plasticity of kitten striate cortex. Science 238: 355–358.
53. Kutsuwada T, Sakimura K, Manabe T, Takayama C, Katakura N, et al. (1996) Impairment of suckling response, trigeminal neuronal pattern formation, and hippocampal LTD in NMDA receptor ε2 subunit mutant mice. Neuron 16: 333–344.
54. Li Y, Erzurumlu RS, Chen C, Jhaveri S, Tonegawa S (1994) Whisker-related neuronal patterns fail to develop in the trigeminal brainstem nuclei of NMDAR1 knockout mice. Cell 76: 427–437.
55. Galvan CD, Hrachovy RA, Smith KL, Swann JW (2000) Blockade of neuronal activity during hippocampal development produces a chronic focal epilepsy in the rat. J Neurosci 20: 2904–2916.
56. Galvan CD, Wenzel JH, Dineley KT, Lam TT, Schwartzkroin PA, et al. (2003) Postsynaptic contributions to hippocampal network hyperexcitability induced by chronic activity blockade in vivo. Eur J Neurosci 18: 1861–1872.

57. Debanne D, Gähwiler BH, Thompson SM (1998) Long-term synaptic plasticity between pairs of individual CA3 pyramidal cells in rat hippocampal slice cultures. J Physiol 507: 237–247.
58. Lubenov EV, Siapas AG (2008) Decoupling through synchrony in neuronal circuits with propagation delays. Neuron 58: 118–131.
59. Huang CS, Shi SH, Ule J, Ruggiu M, Barker LA, et al. (2005) Common molecular pathways mediate long-term potentiation of synaptic excitation and slow synaptic inhibition. Cell 123: 105–118.
60. Fan Y, Fricker D, Brager DH, Chen X, Lu HC, et al. (2005) Activity-dependent decrease of excitability in rat hippocampal neurons through increases in I(h). Nat Neurosci 8: 1542–1551.
61. Colgin LL, Jia Y, Sabatier J-M, Lynch G (2005) Blockade of NMDA receptors enhances spontaneous sharp waves in rat hippocampal slices. Neurosci Lett 385: 46–51.

Cell Transplantation, Vol. 18, pp. 381–389, 2009
Printed in the USA.

0963-6897/09 $90.00 + .00
E-ISSN 1555-3892
www.cognizantcommunication.com

ERas Is Expressed in Primate Embryonic Stem Cells But Not Related to Tumorigenesis

Yujiro Tanaka,*¶[1] Tamako Ikeda,*[1] Yukiko Kishi,* Shigeo Masuda,* Hiroaki Shibata,*‡ Kengo Takeuchi,§ Makoto Komura,¶ Tadashi Iwanaka,¶ Shin-ichi Muramatsu,† Yasushi Kondo,# Kazutoshi Takahashi,** Shinya Yamanaka,** and Yutaka Hanazono*

*Division of Regenerative Medicine, Center for Molecular Medicine, Jichi Medical University, Tochigi, Japan
†Division of Neurology, Department of Internal Medicine, Jichi Medical University, Tochigi, Japan
‡Tsukuba Primate Research Center, National Institute of Biomedical Innovation, Ibaraki, Japan
§Department of Pathology, Cancer Institute Hospital, Tokyo, Japan
¶Department of Pediatric Surgery, Graduate School of Medicine, University of Tokyo, Tokyo, Japan
#Mitsubishi Tanabe Pharma, Osaka, Japan
**Center for iPS Cell Research and Application, Institute for Integrated Cell-Material Sciences, Kyoto University, Kyoto, Japan

The ERas gene promotes the proliferation of and formation of teratomas by mouse embryonic stem (ES) cells. However, its human orthologue is not expressed in human ES cells. This implies that the behavior of transplanted mouse ES cells would not accurately reflect the behavior of transplanted human ES cells and that the use of nonhuman primate models might be more appropriate to demonstrate the safety of human ES cell-based therapies. However, the expression of the ERas gene has not been examined in nonhuman primate ES cells. In this study, we cloned the cynomolgus homologue and showed that the ERas gene is expressed in cynomolgus ES cells. Notably, it is also expressed in cynomolgus ES cell-derived differentiated progeny as well as cynomolgus adult tissues. The ERas protein is detectable in various cynomolgus tissues as assessed by immunohistochemisty. Cynomolgus ES cell-derived teratoma cells, which also expressed the ERas gene at higher levels than the undifferentiated cynomolgus ES cells, did not develop tumors in NOD/Shi-*scid*, IL-2Rγ^{null} (NOG) mice. Even when the ERas gene was overexpressed in cynomolgus stromal cells, only the plating efficiency was improved and the proliferation was not promoted. Thus, it is unlikely that ERas contributes to the tumorigenicity of cynomolgus cells. Therefore, cynomolgus ES cells are more similar to human than mouse ES cells despite that ERas is expressed in cynomolgus and mouse ES cells but not in human ES cells.

Key words: Embryonic stem cell; ERas; Cynomolgus monkey; Tumorigenesis

INTRODUCTION

The ERas gene promotes the growth of and formation of teratomas by mouse ES cells by producing a constitutively active ERas protein and is not expressed in mouse ES cell-derived differentiated progeny or mouse tissues (22). Disruption of the ERas gene in mouse ES cells by homologous recombination results in a significantly reduced proliferation rate and a reduced tumorigenic potential without loss of pluripotency (22). Although the ERas gene is expressed in divergent species such as mice, dogs, and cows, it is not expressed in humans (1,12,17). Its inactivation is likely a relatively recent event in mammalian evolution. It is intriguing to speculate that some of the differences in the proliferation rate or other properties of mouse and human ES cells (9,13) are related to the differences in expression of this constitutively active ERas gene. It may also imply that the behavior of transplanted mouse ES cells does not accurately reflect the behavior of transplanted human ES cells and that the use of nonhuman primate models (11,21,25) would be more appropriate to demonstrate the safety (tumorigenicity) of human ES cell-based therapies (12). However, the expression of the ERas gene has not been examined in nonhuman primate ES cells (19,24). Here, we show that the ERas gene is expressed

Received July 18, 2008; final acceptance October 21, 2008. Online prepub date: April 15, 2009.
[1]Equal contribution.
Address correspondence to Yutaka Hanazono, M.D., Ph.D., Professor, Division of Regenerative Medicine, Center for Molecular Medicine, Jichi Medical University, 3311-1 Yakushiji, Shimotsuke, Tochigi 329-0498, Japan. Tel: +81-285-58-7451; Fax: +81-285-44-5205; E-mail: hanazono@jichi.ac.jp

in cynomolgus ES cells unlike human ES cells. In addition, the ERas gene is widely expressed in adult cynomolgus tissues. However, its forced expression in cynomolgus cells even at high levels was not related to tumorigenesis. Therefore, cynomolgus ES cells are more similar to human than mouse ES cells despite that ERas is expressed in cynomolgus and mouse ES cells but not in human ES cells.

MATERIALS AND METHODS

Cell Culture and Differentiation

A cynomolgus ES cell line (CMK6) (19), its subline (CMK6G) stably expressing enhanced green fluorescent protein (EGFP) (20), and a human ES cell line (SA181, Cellartis AB, Göteborg, Sweden) (10) were maintained on a feeder layer of mitomycin C (Kyowa, Tokyo, Japan)-treated mouse (BALB/c, Clea, Tokyo, Japan) embryonic fibroblasts (MEFs) as previously described (10,19). Confluent ES cells were dissociated from the feeder layer using 0.1% collagenase type IV (Invitrogen, Carlsbad, CA, USA). Cynomolgus stromal cells were obtained from cultured adherent cells of cynomolgus bone marrow.

For neural differentiation from cynomolgus ES cells, astrocyte-conditioned medium (ACM) was prepared by culturing astrocytes obtained from mouse fetal cerebra in Dulbecco's modified Eagle's medium (DMEM)/F12 medium containing an N2 supplement (Invitrogen) (15). Colonies of cynomolgus ES cells (800–1000 μm in diameter) were plucked from the feeder layer using a glass capillary and transferred into nonadhesive bacteriological dishes each containing ACM supplemented with 20 ng/ml of recombinant human fibroblast growth factor-2 (FGF-2) (R&D, Minneapolis, MN, USA). The colonies were cultured for 12 days, giving rise to neural stem cells, which were plated onto poly-L-lysine/laminin (Sigma-Aldrich, St. Louis, MO, USA)-coated dishes and cultivated for 7 days in Neurobasal medium supplemented with 2% B-27 (both from Invitrogen), 20 ng/ml of FGF-2, and 20 ng/ml of recombinant human epidermal growth factor (R&D). After the medium was replaced with ACM and 14 days of culture, the neural stem cells differentiated into neurons (16).

ERas Cloning and Transfection

Based on the human ERas cDNA sequence in Genbank (accession No. NM 181532), the primer set 5′-CAT GGA GCT GCC AAC AAA GCC TG-3′ and 5′-TGT GTC CCT CAA AGC TAG TTG CCT-3′ was designed for the cynomolgus ERas' complete coding sequence. Total RNA was extracted from cynomolgus ES cells using the EZ1 RNA universal tissue kit (Qiagen, Hilden, Germany) with RNase-Free DNase Set (Qiagen), and reverse-transcribed using the RNA LA PCR kit (Takara, Shiga, Japan) with an oligo dT primer. The resulting cDNA was subjected to PCR with this primer set. The PCR product was sequenced with the ABI Prism 310 (Applied Biosystems, Foster, CA, USA). The sequence analysis was performed with Genetyx-Mac software (Genetyx Corporation, Tokyo, Japan). We previously constructed the plasmids pPyCAG-EGFP-gw-IP (expressing EGFP) and pPyCAG-EGFP-gw-IP-mouse ERas (expressing EGFP-mERas) (22). The cDNA encoding the human or cynomolgus ERas gene was inserted into pPyCAG-EGFP-gw-IP to construct pPyCAG-EGFP-gw-IP-human ERas (expressing EGFP-human ERas) or pPyCAG-EGFP-gw-IP-cynomolgus ERas (expressing EGFP-cynomolgus ERas), respectively. The insert was confirmed by DNA sequencing. The plasmids were transfected into cynomolgus stromal cells using Lipofectamin 2000 (Invitrogen). The transfected cells were selected in the presence of puromycin (5 μg/ml).

Transplantation

Cells (1×10^7/site) were transplanted into the thigh muscle of immunodeficient NOD/Shi-*scid*, IL-2Rγ^{null} (NOG) mice which were purchased from Central Institute for Experimental Animals (Kanagawa, Japan). Cynomolgus ES cell-derived teratomas were generated after in utero transplantation of cynomolgus ES cells into fetal sheep as described previously (23). Adherent cells from the teratomas were propagated in DMEM (Sigma-Aldrich) supplemented with 10% fetal bovine serum (FBS) (HyClone, Logan, UT, USA). All experiments were performed in accordance with the Jichi Medical University Guide for Laboratory Animals. Experimental procedures were approved by the Animal Care and Use Committee of Jichi Medical University.

Reverse Transcription (RT)-PCR

cDNA was prepared from each sample as mentioned above and subjected to PCR with the following primer sets: for Oct-4, 5′-GGA CAC CTG GCT TCG GAT T-3′ and 5′-TTC GCT TTC TCT TTC GGG C-3′; and for glyceraldehyde-3-phosphate dehydrogenase (GAPDH), 5′-CCC TGG CCA AGG TCA TCC ATG ACA AC-3′ and 5′-CCA GTG AGC TTC CCG TTC AG-3′. Amplification conditions were 30 cycles of 95°C for 60 s, 58°C for 60 s, and 72°C for 60 s. PCR without the initial RT was also conducted to rule out DNA contamination. For real-time quantitative RT-PCR, a QuantiTect SYBR Green PCR kit (Qiagen) and the ABI Prism 7000 (Applied Biosystems) were used, and amplification conditions were 40 cycles of 95°C for 60 s, 58°C for 60 s, and 72°C for 60 s. The gene expression levels were adjusted based on those of the internal control GAPDH.

Immunoblotting

Preparation of cell lysates and Western blot analyses were performed as described previously (22). Briefly, cells (1×10^7) were washed twice with ice-cold phosphate-buffered saline (PBS) and suspended in the buffer containing 10 mM Tris-HCl (pH 7.5), 1 mM $MgCl_2$, and the 1× Complete Protease Inhibitors (Roche, Basel, Switzerland), followed by incubation on ice for 30 min. These samples were disrupted with Dounce tissue homogenizer (Wheaton, NJ, USA) and added with 1 M NaCl to a final concentration of 150 mM. For lysis, these samples were added with a final concentration of 5% SDS, 1% NP-40, and 1% deoxicorate acids, followed by incubation on ice for 10 min. The samples were then centrifuged at $12,000 \times g$ for 30 min at 4°C, and supernatants were collected. The protein concentrations were measured by the Bio-Rad Bradford assay (BioRad Laboratories, CA, USA). An equal amount of protein (10 μg per lane) was electrophoresed on 12.5% polyacrylamide gel (Atto, Tokyo, Japan) and blotted onto a PVDF membrane (Immobiron; Millipore, MA, USA). The membrane was blocked by TBST containing 5% w/v Amersham ECL-Blocking Agent (GE Healthcare, Buckinghamshire, UK) and then incubated with rabbit antiserum against mouse ERas (22) overnight at 4°C. After washed with TBST, the membrane was incubated with anti-rabbit IgG HRP (Jackson Laboratory, CA, USA) at room temperature for 60 min. Signal was detected using Amersham ECL Plus Western Blotting Detection reagents (GE Healthcare) according to the manufacturer's protocol and visualized on the LAS 3000 mini (Fujifilm, Tokyo, Japan).

Immunohistochemistry

For the immunofluorescent staining of frozen sections, tissues were fixed with 4% paraformaldehyde. The sections were labeled with rabbit anti-serum against mouse ERas (22). The primary antibody (Ab) was detected with a Tyramide Signal Amplification Kit (Invitrogen). After nuclei were stained with DAPI (Donjindo, Kumamoto, Japan), the sections were observed with a confocal laser scanning microscope (Olympus, Tokyo, Japan). For immunohistochemistry, tissues were fixed with 4% paraformaldehyde and embedded in paraffin. To identify GFP-positive cells, the sections were stained with rabbit anti-GFP Ab (Clontech, Palo Alto, CA, USA), reacted with the Dako EnVision+ System HRP (Dako, Copenhagen, Denmark), and visualized with 3,3′-diaminobenzide tetrahydrochloride (Dojindo). Nuclei were counterstained with hematoxylin.

Flow Cytometry

The expression of GFP and ERas was analyzed using a FACS Calibur flow cytometer (BD Pharmingen, San Diego, CA, USA). To detect ERas, cells were fixed using fixation/permeabilization buffer (eBioscience, San Diego, CA, USA) for 2 h at 4°C and then incubated with Alexa Fluor 647 (Invitrogen)-conjugated rabbit antiserum against ERas for 60 min at 4°C. Data acquisition and analysis were performed using CellQuest software (BD Pharmingen). Fluorescence-conjugated, irrelevant Abs served as negative controls.

Cell Proliferation Assay

Total cell numbers and proliferating cell numbers were measured with Cell Counting Kit-8 (Dojindo) and with Cell Proliferation ELISA, BrdU (colorimetric) (Roche), respectively. For Cell Counting Kit-8, cells were seeded in 96-well plates at 5×10^3 per well and measured after 6, 24, 36, 48, and 80 h of incubation according to the manufacturer's instructions. For Cell Proliferation ELISA, cells were seeded in 96-well plates at 2×10^3 per well and measured after 24, 36, 48, 72, and 96 h of incubation. Significant differences were examined using the *t*-test.

RESULTS AND DISCUSSION

Cynomolgus Cells and Tissues Express ERas

We first cloned and sequenced the cynomolgus orthologue of the ERas gene from cDNA of the undifferentiated cynomolgus ES cells (Fig. 1A). The translated amino acid sequence showed a higher degree of homology to human than mouse ERas (99% vs. 75%) (Fig. 1B). We could not detect the ERas protein in cynomolgus ES cells by flow cytometry, implying its weak expression (data not shown).

Next, we examined the expression of the ERas gene in adult cynomolgus tissues by RT-PCR. Using a primer set to cover the entire coding region, the amplicons from all nine somatic tissues were the same size as that from cynomolgus ES cells (Fig. 2A). The PCR product was sequenced to confirm that it was the ERas gene. This clearly shows that a full-length version of the ERas gene is transcribed in cynomolgus tissues, despite that ERas is not expressed in mouse tissues (22).

We then examined the protein expression in adult cynomolgus tissues by immunohistochemistry. Immunoblotting revealed that the antibody reacts to human and cynomolgus ERas as well as mouse ERas, although the antibody was generated against recombinant mouse ERas (22) (Fig. 2B). In addition, it specifically reacts to ERas (25 kDa) and does not react to other Ras family proteins (N-, H-, or K-Ras; 21 kDa) in cynomolgus cells expressing these Ras genes (Fig. 2B). Using this antibody, we detected ERas-positive cells in all tissues tested (brain, thymus, intestine, and ovary) (Fig. 2C). At a higher magnification, it turned out that ERas is localized on the cytoplasmic membrane as expected (Fig.

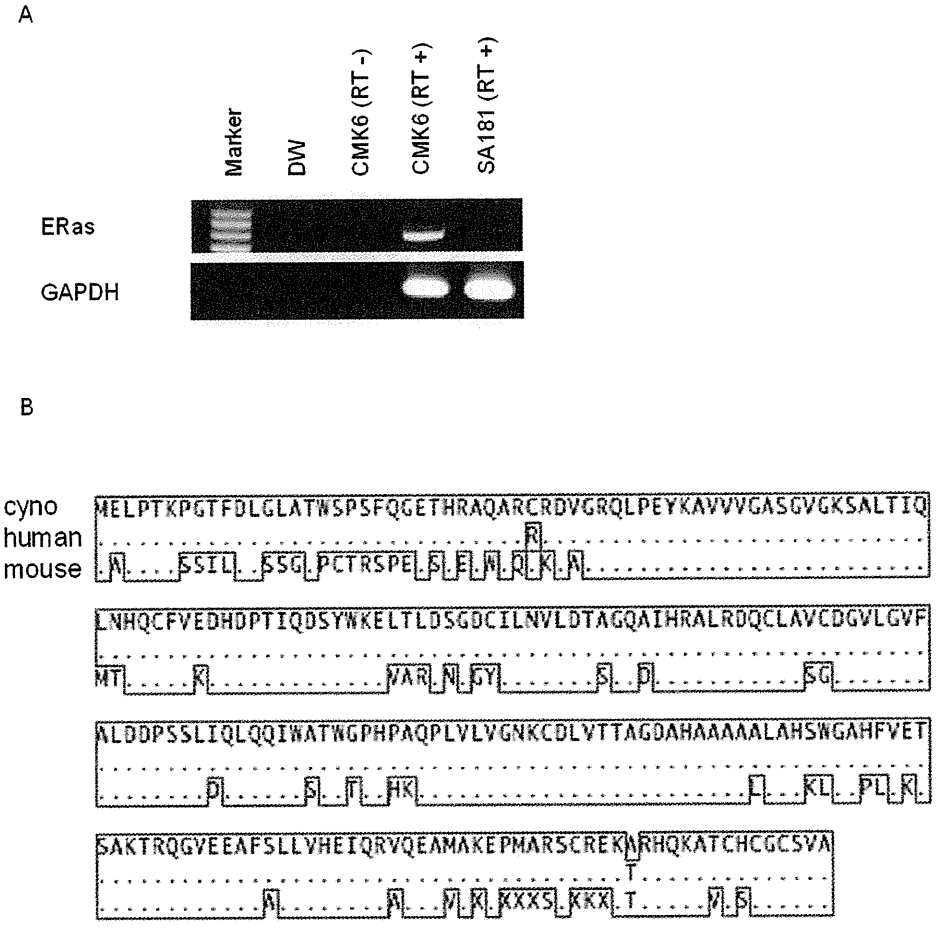

Figure 1. Cloning and sequencing of cynomolgus ERas. (A) The expression of the cynomolgus (cyno) ERas gene is detectable in cynomolgus ES cells (CMK6), but not in human ES cells (SA181), by reverse transcription (RT)-PCR. To exclude the possibility of genomic DNA contamination, PCR without the RT procedure (designated RT −) was also conducted. DW (distilled water) indicates no template in the reaction. RT-PCR of the GAPDH sequence is also shown as an internal control. (B) Amino acid sequences of cynomolgus, human (accession No. NM 181532), and mouse (accession No. NM 181548) ERas are shown. Amino acids identical to cynomolgus ERas are shown as dots and conserved amino acids are encircled with a solid line.

2D). We also tested mouse tissues, but ERas-positive cells were not detectable (Fig. 2C). Taken together, the ERas protein is indeed expressed in cynomolgus tissues, unlike in murine tissues.

The expression of the ERas gene becomes undetectable after the differentiation of mouse ES cells (22). We examined the expression of the ERas gene after the differentiation of cynomolgus ES cells. Cynomolgus ES cell-derived neurons and teratoma cells were examined for the expression of ERas as well as Oct-4, a pluripotent marker of ES cells. They were positive for ERas but negative for Oct-4 (Fig. 3A). Although cynomolgus ES cell-derived neurons were fragile and scarcely survived after dissociation from the culture dish, adherent teratoma cells could be cultured for more than six passages at a dilution of 1:4 to 1:8. Quantitative RT-PCR showed that the ERas gene expression levels were even higher in the cultured teratoma cells than in the undifferentiated cynomolgus ES cells (Fig. 3B). Then, we transplanted 1×10^7 cultured teratoma cells expressing the ERas gene (GFP-positive, passage 3) into the thigh muscle of NOG mice ($n = 3$), and examined the tumorigenicity of the cells. NOG mice were used as recipients, because they are more immunodeficient than other immunodeficient mice and transplanting to NOG mice is the most sensitive assay to detect tumorigenesis (7,14). However, no tumor developed after 2.5 months, although the transplanted cell progeny (GFP positive) were detected in every specimen (Fig. 3C). On the other hand, undifferentiated cynomolgus ES cells formed tera-

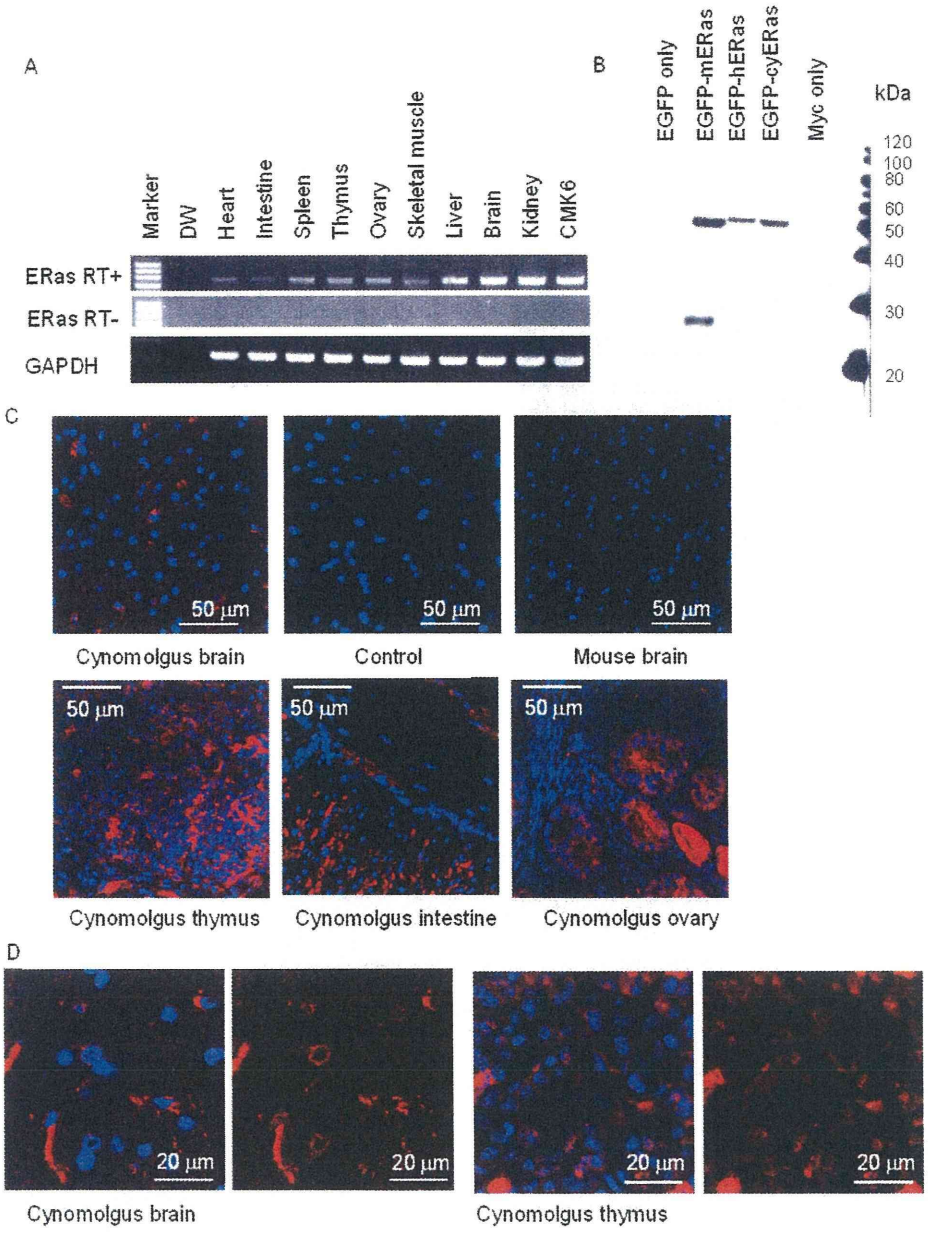

Figure 2. Cynomolgus tissues express ERas. (A) The expression of the cynomolgus ERas gene is detectable in various cynomolgus tissues by RT-PCR. To exclude the possibility of genomic DNA contamination, PCR without the RT procedure (designated RT –) was also conducted. DW indicates no template in the reaction. RT-PCR of the GAPDH sequence is also shown as an internal control. (B) Cynomolgus bone marrow stromal cells were transfected with the mouse ERas (mERas), human ERas (hERas), or cynomogus ERas (cyERas) gene fused with the EGFP gene, and immnunoblotted with the polyconal anti-ERas antibody. Although the antibody was generated against recombinant mERas (22), it reacts to hERas and cyERas as well as mERas. In addition, it does not react to cynomolgus other Ras family proteins (N-, H-, or K-Ras; 21 kDa). ERas (25 kDa) fused with EGFP (26 kDa) is detectable at 51 kDa. In mERas-transfected cells, ERas alone released from the fusion protein was also detected. (C) Using the anti-ERas antibody, ERas-positive cells (red) were detected in cynomolgus brain, thymus, intestine, and ovary. Control indicates the staining of cynomolgus brain without the primary ERas antibody. Although the primary antibody to ERas was originally developed for mouse ERas and should react more strongly to mouse than cynomolgus ERas, no positive signals were detected in mouse brain. (D) The ERas fluorescence with or without DAPI is shown at a higher magnification of both cynomolgus brain and thymus. ERas was detected on the cytoplasmic membrane.

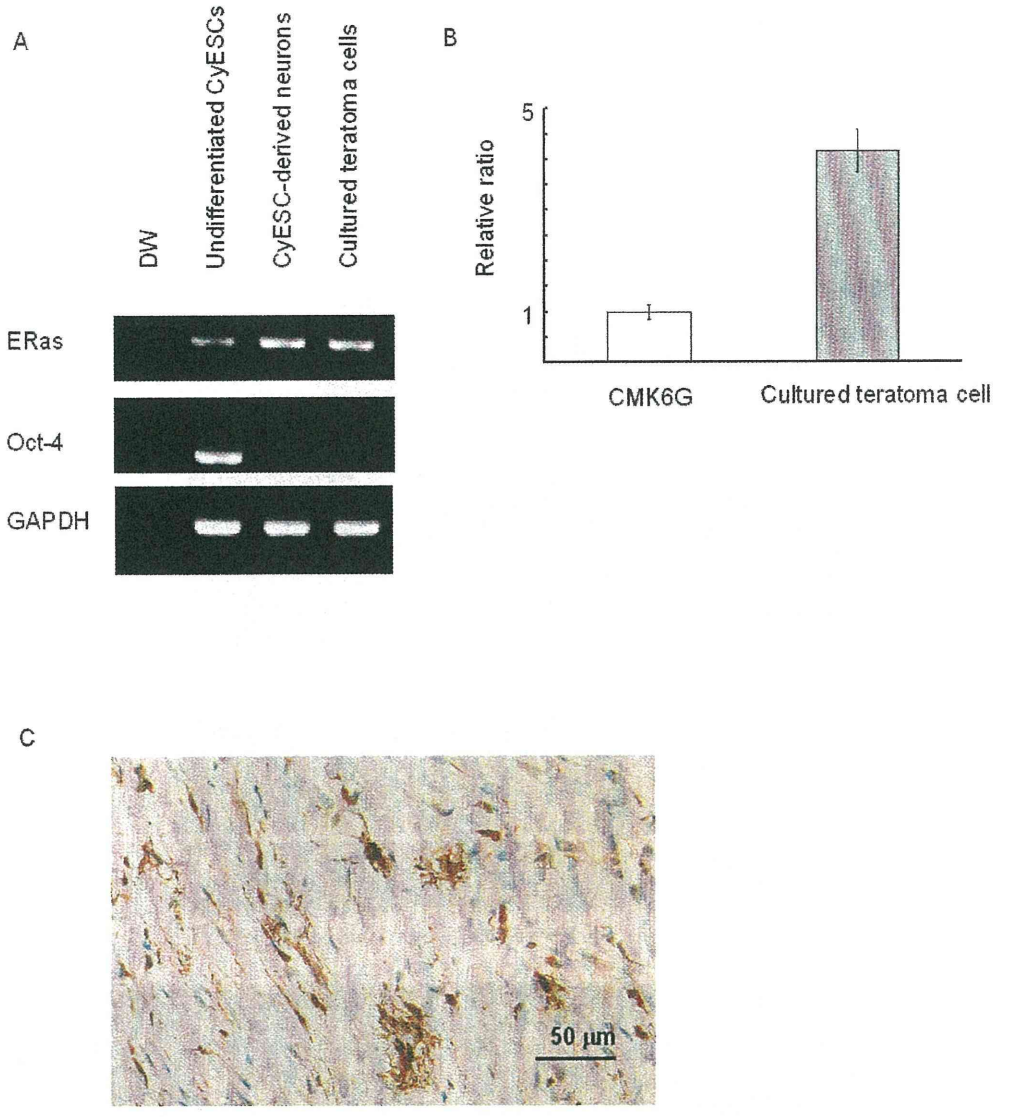

Figure 3. Cynomolgus ES cell-derived cells express ERas but do not form tumors in vivo. (A) The ERas gene was expressed in cynomolgus ES cell-derived neurons and teratoma cells as assessed by RT-PCR, whereas the Oct-4 gene was expressed in neither. DW indicates no template in the reaction. RT-PCR of the GAPDH sequence is also shown as an internal control. (B) The ERas gene expression level was nearly five times higher in the cultured teratoma cells than in the undifferentiated cynomolgus ES cells as assessed by quantitative RT-PCR. The gene expression level was adjusted using the internal control GAPDH. (C) The cultured teratoma cells were transplanted into the thigh muscles of NOG mice and examined for tumorigenicity in vivo after 2.5 months. Staining of the specimen with anti-GFP is shown. Although the transplanted cell progeny (GFP positive, brown) were detected, no tumor was observed.

tomas in all NOG mice. Taken together, cynomolgus ES cell-derived differentiated progeny and teratoma cells also express the ERas gene, but do not produce tumors in vivo.

ERas Overexpression in Cynomolgus Cells

To examine whether the cynomolgus ERas contributes to cell proliferation, we transfected cynomolgus stromal cells with a plamid expressing the cynomolgus or mouse ERas, EGFP, and puromycin resistance genes. Transfectants were obtained by treatment with puromycin and more than 90% of the cells expressed EGFP (Fig. 4A). These transfectants did not show significant morphological changes. Quantitative RT-PCR showed that the transfected cells expressed approximately 1000 times more ERas than undifferentiated cynomolgus ES

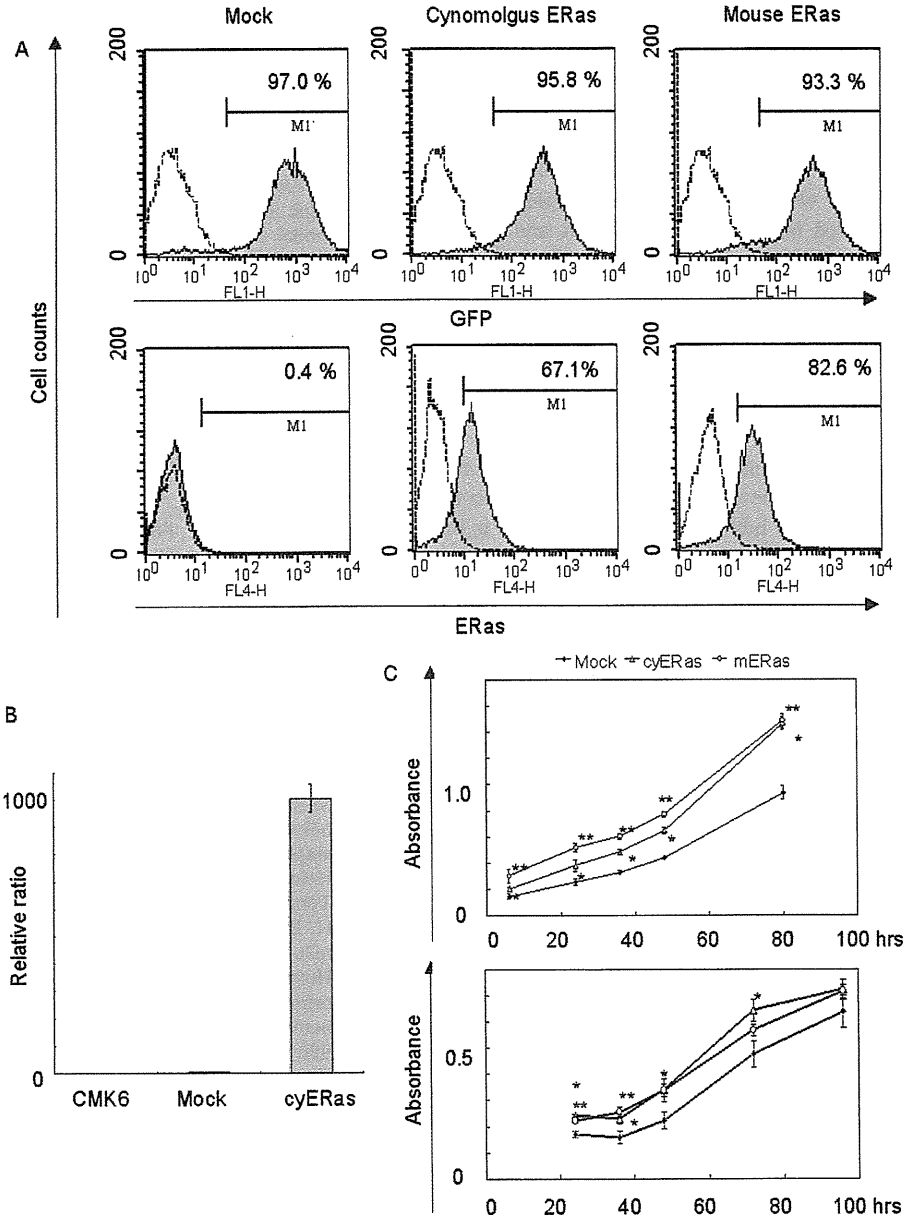

Figure 4. Overexpression of ERas does not promote cell proliferation but improves plating efficiency. (A) The plasmids expressing the cynomolgus or mouse ERas, EGFP, and puromycin resistance genes were transfected into cynomolgus stromal cells. After puromycin selection, more than 90% of cells expressed EGFP (upper). The ERas expression was also detected by flow cytometry (lower). (B) The level of cynomolgus ERas gene expression was 1000 times higher in the cynomolgus ERas-transfected cells (cyERas) than in naive cynomolgus ES cells (CMK6) or mock-transfected cells by quantitative RT-PCR. The gene expression levels were adjusted using the internal control GAPDH. (C) The mock-, cynomolgus ERas (cyERas)-, and mouse ERas (mERas)-transfected cells were plated at 5×10^3 per well and total cell numbers were measured after 6, 24, 36, 48, and 80 h of incubation (upper). The mock-, cyERas-, and mERas-transfected cells were plated at 2×10^3 per well and proliferating cell numbers were measured after 24, 36, 48, 72, and 96 h of incubation (lower). The cyERas- and mERas-transfected cells showed larger total cell or proliferating cell numbers after plating than the mock-transfected cells, but did not show any more rapid proliferation thereafter. Statistical differences with the *t*-test are indicated: $*p < 0.01$ for the cyERas- versus mock-transfected cells, $**p < 0.01$ for the mERas- versus mock-transfected cells.

cells (Fig. 4B). These cells expressing either cynomolgus or mouse ERas showed larger total cell numbers or proliferating cell numbers after plating than the mock-transfected cells, but did not show any more rapid proliferation thereafter (Fig. 4C). Thus, cynomolgus ERas improves plating efficiency but does not promote cell proliferation, even when it is expressed at high levels.

In this report, we showed that the cynomolgus ERas gene is expressed in cynomolgus ES cells and tissues. Its expression pattern is quite different from that of mouse ERas, which is not expressed in mouse ES cell-derived differentiated progeny or mouse tissues. Although cynomolgus ERas improved the plating efficiency when overexpressed, its expression did not promote cell proliferation or induce tumor formation in vivo (Figs. 3C, 4C). Thus, cynomolgus ERas might only suppress the apoptosis of cynomolgus cells (5). Because the formation of teratomas is one of the greatest obstacles to the clinical application of human ES cells (3,8,18), it is important to elucidate whether the ERas gene expressed in cynomolgus ES cells is related to teratoma development in vivo in order to tell whether nonhuman primate models are really suitable for preclinical research. From our study, it is at least suggested that cynomolgus ES cells are more similar to human than mouse ES cells in that ERas does not contribute to the formation of teratomas in vivo.

To date, the pluripotent marker Oct-4 has been used to predict the formation of teratomas (4) and the removal of Oct-4-positive cells from ES cell-derived progenitor preparations is reported to prevent teratomas from developing posttransplant (2). However, Oct-4-negative immature cells are also reported to contribute to the formation of teratomas (6). Therefore, although Oct-4 could be used to predict whether teratomas develop to some extent, it does not regulate the developmental process. For future clinical applications, the mechanism by which primate ES cells form teratomas should be studied in more detail.

ACKNOWLEDGMENTS: We thank Naomi Takino for technical assistance and Shuh-hei Fujishiro for helpful discussion. This study was supported by grants (JMS 21st Century COE Program, High-tech Research Center Program, and KAKENHI) from the Ministry of Education, Culture, Sports, Science and Technology of Japan as well as grants (KAKENHI) from the Ministry of Health, Labor and Welfare of Japan.

REFERENCES

1. Bhattacharya, B.; Miura, T.; Brandenberger, R.; Mejido, J.; Luo, Y.; Yang, A. X.; Joshi, B. H.; Ginis, I.; Thies, R. S.; Amit, M.; Lyons, I.; Condie, B. G.; Itskovitz-Eldor, J.; Rao, M. S.; Puri, R. K. Gene expression in human embryonic stem cell lines: unique molecular signature. Blood 103:2956–2964; 2004.
2. Bieberich, E.; Silva, J.; Wang, G.; Krishnamurthy, K.; Condie, B. G. Selective apoptosis of pluripotent mouse and human stem cells by novel ceramide analogues prevents teratoma formation and enriches for neural precursors in ES cell-derived neural transplants. J. Cell Biol. 167:723–734; 2004.
3. Bjorklund, L. M.; Sanchez-Pernaute, R.; Chung, S.; Andersson, T.; Chen, I. Y.; McNaught, K. S.; Brownell, A. L.; Jenkins, B. G.; Wahlestedt, C.; Kim, K. S.; Isacson, O. Embryonic stem cells develop into functional dopaminergic neurons after transplantation in a Parkinson rat model. Proc. Natl. Acad. Sci. USA 99:2344–2349; 2002.
4. Campbell, P. A.; Perez-Iratxeta, C.; Andrade-Navarro, M. A.; Rudnicki, M. A. Oct4 targets regulatory nodes to modulate stem cell function. PLoS ONE 2:e553; 2007.
5. Cox, A. D.; Der, C. J. The dark side of Ras: Regulation of apoptosis. Oncogene 22:8999–9006; 2003.
6. Dihne, M.; Bernreuther, C.; Hagel, C.; Wesche, K. O.; Schachner, M. Embryonic stem cell-derived neuronally committed precursor cells with reduced teratoma formation after transplantation into the lesioned adult mouse brain. Stem Cells 24:1458–1466; 2006.
7. Erdo, F.; Buhrle, C.; Blunk, J.; Hoehn, M.; Xia, Y.; Fleischmann, B.; Focking, M.; Kustermann, E.; Kolossov, E.; Hescheler, J.; Hossmann, K. A.; Trapp, T. Host-dependent tumorigenesis of embryonic stem cell transplantation in experimental stroke. J. Cereb. Blood Flow Metab. 23: 780–785; 2003.
8. Fujikawa, T.; Oh, S. H.; Pi, L.; Hatch, H. M.; Shupe, T.; Petersen, B. E. Teratoma formation leads to failure of treatment for type I diabetes using embryonic stem cell-derived insulin-producing cells. Am. J. Pathol. 166:1781–1791; 2005.
9. Hasegawa, K.; Fujioka, T.; Nakamura, Y.; Nakatsuji, N.; Suemori, H. A method for the selection of human embryonic stem cell sublines with high replating efficiency after single-cell dissociation. Stem Cells 24:2649–2660; 2006.
10. Heins, N.; Englund, M. C.; Sjoblom, C.; Dahl, U.; Tonning, A.; Bergh, C.; Lindahl, A.; Hanson, C.; Semb, H. Derivation, characterization, and differentiation of human embryonic stem cells. Stem Cells 22:367–376; 2004.
11. Hematti, P.; Obrtlikova, P.; Kaufman, D. S. Nonhuman primate embryonic stem cells as a preclinical model for hematopoietic and vascular repair. Exp. Hematol. 33:980–986; 2005.
12. Kameda, T.; Thomson, J. A. Human ERas gene has an upstream premature polyadenylation signal that results in a truncated, noncoding transcript. Stem Cells 23:1535–1540; 2005.
13. Kaufman, D. S.; Thomson, J. A. Human ES cells—haematopoiesis and transplantation strategies. J. Anat. 200: 243–248; 2002.
14. Kishi, Y.; Tanaka, Y.; Shibata, H.; Nakamura, S.; Takeuchi, K.; Masuda, S.; Ikeda, T.; Muramatsu, S.; Hanazono, Y. Variation in the incidence of teratomas after transplantation of nonhuman primate ES cells into immunodeficient mice. Cell Transplant. 17(9):1095–1102; 2008.
15. Nakayama, T.; Momoki-Soga, T.; Inoue, N. Astrocyte-derived factors instruct differentiation of embryonic stem cells into neurons. Neurosci. Res. 46:241–249; 2003.
16. Nakayama, T.; Momoki-Soga, T.; Yamaguchi, K.; Inoue, N. Efficient production of neural stem cells and neurons from embryonic stem cells. Neuroreport 15:487–491; 2004.
17. Rao, M. Conserved and divergent paths that regulate self-

renewal in mouse and human embryonic stem cells. Dev. Biol. 275:269–286; 2004.
18. Shibata, H.; Ageyama, N.; Tanaka, Y.; Kishi, Y.; Sasaki, K.; Nakamura, S.; Muramatsu, S.; Hayashi, S.; Kitano, Y.; Terao, K.; Hanazono, Y. Improved safety of hematopoietic transplantation with monkey embryonic stem cells in the allogeneic setting. Stem Cells 24:1450–1457; 2006.
19. Suemori, H.; Tada, T.; Torii, R.; Hosoi, Y.; Kobayashi, K.; Imahie, H.; Kondo, Y.; Iritani, A.; Nakatsuji, N. Establishment of embryonic stem cell lines from cynomolgus monkey blastocysts produced by IVF or ICSI. Dev. Dyn. 222:273–279; 2001.
20. Takada, T.; Suzuki, Y.; Kondo, Y.; Kadota, N.; Kobayashi, K.; Nito, S.; Kimura, H.; Torii, R. Monkey embryonic stem cell lines expressing green fluorescent protein. Cell Transplant. 11:631–635; 2002.
21. Takagi, Y.; Takahashi, J.; Saiki, H.; Morizane, A.; Hayashi, T.; Kishi, Y.; Fukuda, H.; Okamoto, Y.; Koyanagi, M.; Ideguchi, M.; Hayashi, H.; Imazato, T.; Kawasaki, H.; Suemori, H.; Omachi, S.; Iida, H.; Itoh, N.; Nakatsuji, N.; Sasai, Y.; Hashimoto, N. Dopaminergic neurons generated from monkey embryonic stem cells function in a Parkinson primate model. J. Clin. Invest. 115:102–109; 2005.
22. Takahashi, K.; Mitsui, K.; Yamanaka, S. Role of ERas in promoting tumour-like properties in mouse embryonic stem cells. Nature 423:541–545; 2003.
23. Tanaka, Y.; Nakamura, S.; Shibata, H.; Kishi, Y.; Ikeda, T.; Masuda, S.; Sasaki, K.; Abe, T.; Hayashi, S.; Kitano, Y.; Nagao, Y.; Hanazono, Y. Sustained macroscopic engraftment of cynomolgus embryonic stem cells in xenogeneic large animals after in utero transplantation. Stem Cells Dev. 17:367–382; 2008.
24. Thomson, J. A.; Kalishman, J.; Golos, T. G.; Durning, M.; Harris, C. P.; Becker, R. A.; Hearn, J. P. Isolation of a primate embryonic stem cell line. Proc. Natl. Acad. Sci. USA 92:7844–7848; 1995.
25. Wolf, D. P. Nonhuman primate embryonic stem cells: An underutilized resource. Regen. Med. 3:129–131; 2008.

Cardiovascular Research (2009) 83, 682–687
doi:10.1093/cvr/cvp171

The cardiac pacemaker-specific channel *Hcn4* is a direct transcriptional target of MEF2

Shinobu Kuratomi[1], Yoko Ohmori[1], Masayuki Ito[1], Kuniko Shimazaki[1], Shin-ichi Muramatsu[2], Hiroaki Mizukami[3], Hideki Uosaki[4], Jun K. Yamashita[4], Yuji Arai[5], Koichiro Kuwahara[6], and Makoto Takano[1]*

[1]Department of Physiology, School of Medicine, Jichi Medical University, Shimotsuke, Tochigi 329-0498, Japan; [2]Division of Neurology, Department of Medicine, School of Medicine, Jichi Medical University, Shimotsuke, Tochigi 329-0498, Japan; [3]Division of Genetic Therapeutics, Center for Molecular Medicine, Jichi Medical University, Shimotsuke, Tochigi 329-0498, Japan; [4]Laboratory of Stem Cell Differentiation, Stem Cell Research Center, Institute for Frontier Medical Sciences, Kyoto University, Kyoto 606-8507, Japan; [5]Department of Bioscience, National Cardiovascular Center Research Institute, Suita, Osaka 565-8565, Japan; and [6]Department of Medicine and Clinical Sciences, Graduate School of Medicine, Kyoto University, Kyoto 606-8507, Japan

Received 21 January 2009; revised 8 May 2009; accepted 22 May 2009; online publish-ahead-of-print 28 May 2009

Time for primary review: 34 days

KEYWORDS
Hcn4;
MEF2;
Sino-atrial node;
Channel;
Transcription

Aims *Hcn4*, which encodes the hyperpolarization-activated, cyclic nucleotide-sensitive channel (I_h), is a well-established marker of the cardiac sino-atrial node. We aimed to identify *cis*-elements in the genomic locus of the *Hcn4* gene that regulate the transcription of *Hcn4*.

Methods and results We screened evolutionarily conserved non-coding sequences (CNSs) that are often involved in the regulation of gene expression. The VISTA Enhancer Browser identified 16 regions, termed CNS 1-16, within the *Hcn4* locus. Using the luciferase reporter assay in primary neonatal rat cardiomyocytes, we found that CNS13 conferred a prominent enhancer activity (more than 30-fold) on the *Hcn4* promoter. Subsequent mutation analysis revealed that the *Hcn4* enhancer function was dependent on myocyte enhancer factor-2 (MEF2) and activator protein-1 (AP1) binding sequences located in CNS13. Electrophoretic mobility shift assay and chromatin immunoprecipitation confirmed that MEF2 and AP1 proteins bound CNS13. Furthermore, overexpression of a dominant negative MEF2 mutant inhibited the enhancer activity of CNS13, decreased *Hcn4* mRNA expression and also decreased the amplitude of I_h current in myocytes isolated from the inflow tract of embryonic heart.

Conclusion These results suggest that the novel enhancer CNS13 and MEF2 may play a critical role in the transcription of *Hcn4* in the heart.

1. Introduction

The appropriate timing of cardiac muscle contraction is regulated by the electrical conduction system of the heart and consists of cardiomyocytes possessing specialized electrical function. The precise expression pattern of cardiac ion channel genes in relation to such electrophysiological properties has been extensively studied.[1,2] Previous reports have demonstrated that the hyperpolarization-activated, cyclic nucleotide-sensitive cation current (I_h) encoded by the *Hcn4* gene appears one of the ion currents underlying pacemaker depolarization.[3,4] In mammalian adult heart, *Hcn4* is specifically expressed in the sino-atrial node (SAN). During development *Hcn4* is also expressed in the foetal and neonatal chamber myocardium. As a result of this distribution, *Hcn4* is now recognized as a key marker gene of the SAN.[5,6] Despite its role as an SAN marker, little is known about the *cis*-elements that directly regulate *Hcn4* expression. Progress in the genome project and comparative genomic-base approaches have proven useful in the identification of gene regulatory sequences in a wide range of genomic loci.[7,8] We have previously reported that an 847 bp proximal sequence induces minimal promoter activity of the *Hcn4* gene.[9] In addition to this proximal upstream region, we also identified conserved, non-coding sequences within the *Hcn4* gene locus and analysed their enhancer function. We found that the novel enhancer contained binding sites for activator protein-1 (AP1) and myocyte enhancer factor-2 (MEF2) and played a critical role in the expression of *Hcn4*. These results outline the potential mechanisms underlying SAN differentiation.

* Corresponding author. Tel: +81 285 58 7308; Fax: +81 285 40 6294.
E-mail address: takanom@jichi.ac.jp

2. Methods

2.1 Construction of the promoter reporter plasmid

Luciferase reporter constructs were prepared using pGL4.10 vector (Promega) and the *Hcn4* promoter construct was obtained as previously described.[9] Conserved non-coding sequence (CNS) fragments were isolated from mouse genomic DNA by PCR with the primer pairs listed in Supplementary material online, *Table S1* and were subcloned into the upstream region of the *Hcn4* promoter.

2.2 Cell culture

For the culture of neonatal cardiomyocytes, 1- to 2-day-old rats were decapitated, the ventricle rapidly dissected and myocytes isolated by collagenase digestion (Worthington, type 2, 80 U/mL). The myocytes were then enriched by discontinuous Percoll gradient centrifugation (yield more than 90%).

For the culture of embryonic cardiomyocytes, rat embryos (13 days after fertilization) were removed from pregnant rats under deep anaesthesia with ether, the inflow tract of embryonic heart dissected and the primordial right and left appendixes removed. Myocytes were then isolated using the same procedure as that for the culture of neonatal myocytes.

Embryonic and neonatal cardiomyocytes were plated at a density of 2×10^4 and 10^5 cells/well, respectively, in 24-well plates and cultured in DMEM with 10% foetal bovine serum.[9]

All experiments were approved in advance by the animal Ethics Committee of Jichi Medical University. The investigation conforms with the Guide for the Care and Use of Laboratory Animals published by the US National Institutes of Health (NIH Publication No. 85-23, revised 1996).

2.3 Luciferase reporter gene assay

Luciferase reporter constructs (0.5 μg) and pGL4.74 vector (0.03 μg) were co-transfected into neonatal cardiomyocytes using Lipofectamine LTX (Invitrogen). Luciferase activities were measured 3 days after the transfection using the Dual-Luciferase Reporter Assay System (Promega). Transcriptional activities were obtained from three separate assays performed in quadruplicate.

2.4 Electrophoretic mobility shift assays

The myc-tagged mouse c-Jun/AP1 and MEF2C proteins were *in vitro* translated using TNT Quick Coupled Transcription/Translation System (Promega) and CNS13 DNA probes radiolabelled with [^{32}P]. The binding reaction was then performed in a reaction buffer (final volume=20 μL) containing 20 mM HEPES (pH 7.6), 50 mM KCl, 1 mM $MgCl_2$, 0.1% Nonidet P-40, 5% glycerol, 5 mM dithiothreitol, 1 mM EDTA, and 1 μg poly(dI-dC). The probe (10 fmol) incubated with 1 μL of protein was analysed on 4% polyacrylamide gels in ×0.25 TBE buffer. In competition experiments, 100-fold molar excess of double-strand oligonucleotides (AP1: 5′-ATT CTG AGT CAG AGA-3′ and MEF2: 5′-AGG TGG GTT AAA AAT AGA GCC CT-3′) were added.

2.5 Chromatin immunoprecipitation

Chromatin isolated from neonatal rat cardiomyocytes was immunoprecipitated with specific antibodies directed against anti-c-Jun/AP1 (Calbiochem) and anti-MEF2 (AnaSpec) using the EZ chromatin immunoprecipitation (ChIP) assay kit (Upstate) and analysed by PCR using the following primer pairs: CNS13 ChIP primers 5′-CCT TGG TTG TGA GTC TGT GTC T-3′ (forward) and 5′-AGT GGA GAG ACT GCT CTT TTC C-3′ (reverse) and control ChIP primers 5′-AAT GGG ACT CCT CTT ACT CAT TTC T-3′ (forward) and 5′-AAA GTC CCT GAT GAC ACA CTA GTT C-3′ (reverse).

2.6 AAV vector production and transfection

Adeno-associated virus (AAV) vector plasmids contain an expression cassette consisting of a CMV promoter followed by the first intron of human growth hormone, target cDNA, woodchuck hepatitis virus post-transcriptional regulatory element (GenBank accession no. J04514) and the SV40 poly-A signal sequence, between the inverted terminal repeats of the AAV-3 genome. The plasmids pAAV-dnMEF2 and pAAV-GFP contained the cDNA of the dominant negative MEF2 (dnMEF2) fused with Orange fluorescent protein (Clontech) and GFP, respectively. The two helper plasmids, pHelper (Agilent) and pAAV1-RC, harbour the *E2A*, *E4*, and *VA RNA* genes of the adenovirus genome, and the AAV-1 *rep* and *cap* genes, respectively. HEK293 cells were cotransfected using the calcium phosphate coprecipitation method with the vector plasmid, pAAV1-RC and pHelper. AAV1 vectors were harvested and purified via two sequential continuous iodoxale ultracentrifugations. The vector titer was determined by quantitative PCR (Q-PCR) of DNase I-treated vector stocks, yielding 10^{11}–10^{12} vector genome copies (vg).[12] 2×10^4 foetal myocytes were transfected with 10^{10} vg AAV1-dnMEF2 or AAV1-EGFP; and 10^5 vg Empty AV5 vector was also transfected as a helper.

2.7 RT-PCR and Q-PCR analysis

Three days after the transfection of AAV1, total RNA was isolated from primary cultured embryonic myocytes using TRIZOL reagent (Invitrogen). Single-strand cDNA was synthesized using Superscript III (Invitrogen). Q-PCR was carried out with predesigned Taqman Probes for *hcn4*, *hcn2*, *hcn1*, *stars*, and the 18s rRNA, in an ABI Prism 7700 System (Applied Biosystems).

2.8 Immunostaining of cardiomyocytes

Cardiomyocytes were fixed with 4% paraformaldehyde and incubated with primary antibodies directed against HCN4 (1:200 dilution; Chemicon) and actinin (1:750; Monoclonal, Sigma). Following extensive washes, cells were incubated with Alexa Fluor 488-conjugated anti-rabbit or anti-mouse Ig secondary antibodies at a concentration of 1:500 (Molecular Probes).

2.9 Electrophysiological analysis

Electrophysiological measurements were carried out using an Axopatch200B amplifier and a Digidata 1320 interface (Axon). The bathing solution contained 140 mM NaCl, 5.4 mM KCl, 0.33 mM NaH_2PO_4, 0.5 mM $MgCl_2$, 1.8 mM $CaCl_2$, 0.5 mM $BaCl_2$, 5 mM HEPES (pH 7.4 with NaOH), and the standard high K^+ pipette solution contained 110 Aspartic acid, 30 mM KCl, 5 mM MgATP, 5 mM Na_2 creatine phosphate, 0.1 mM Na_2GTP, 2 mM EGTA, 10 mM HEPES (pH 7.2 with KOH).

2.10 Statistical analysis

Data are expressed as mean ± SD values. Statistical analysis was performed using the Student's *t*-test and $P < 0.05$ was defined as statistically significant.

3. Results

3.1 Functional analysis of conserved non-coding regions within the *Hcn4* gene locus

Our previous study revealed that the proximal 847 bp sequence in the *Hcn4* upstream region is essential for promoter activity.[9] In order to locate additional *cis*-regulatory sequences, we extensively searched the CNSs in the genomic locus of *Hcn4*. As illustrated in *Figure 1A*, we identified 16 regions using VISTA Enhancer Browser, and designated these regions CNS 1-16 (Supplementary material online, *Table S1*).[8]

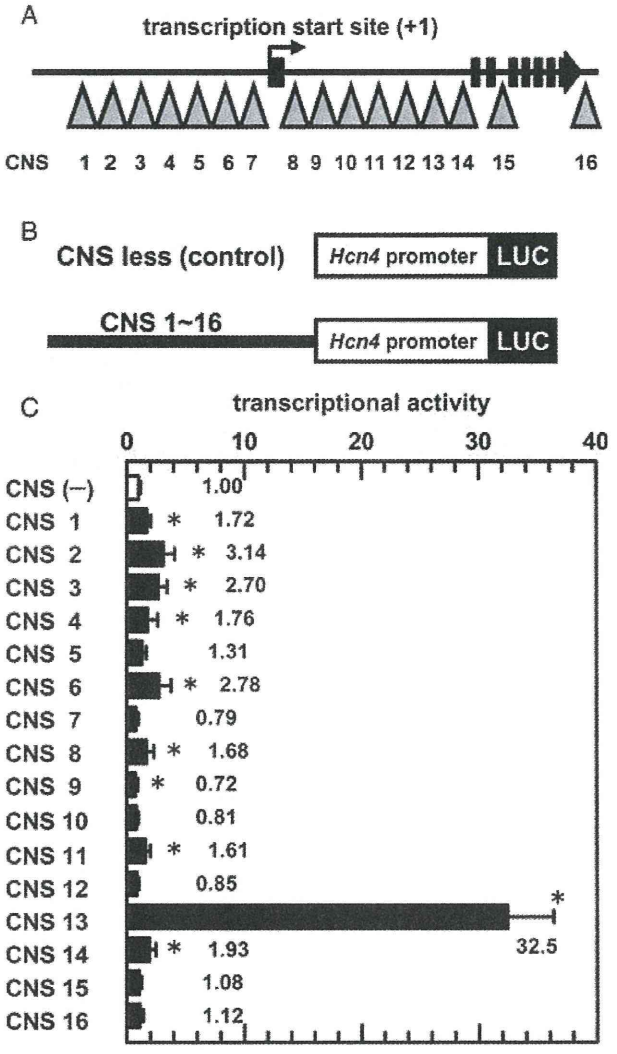

Figure 1 Enhancer activity of the CNS fragments. (*A*) A schematic diagram outlining the genomic organization of the murine *Hcn4* gene. Arrows indicate CNS regions. (*B*) Structure of the luciferase reporter constructs. The *Hcn4* promoter comprises nucleotides −446 to +400 relative to the transcription start site. (*C*) Enhancer activity conferred by the CNS fragments. Data are presented as relative values to the activity of the *Hcn4* promoter. *$P < 0.05$ compared with construct of *Hcn4* promoter alone.

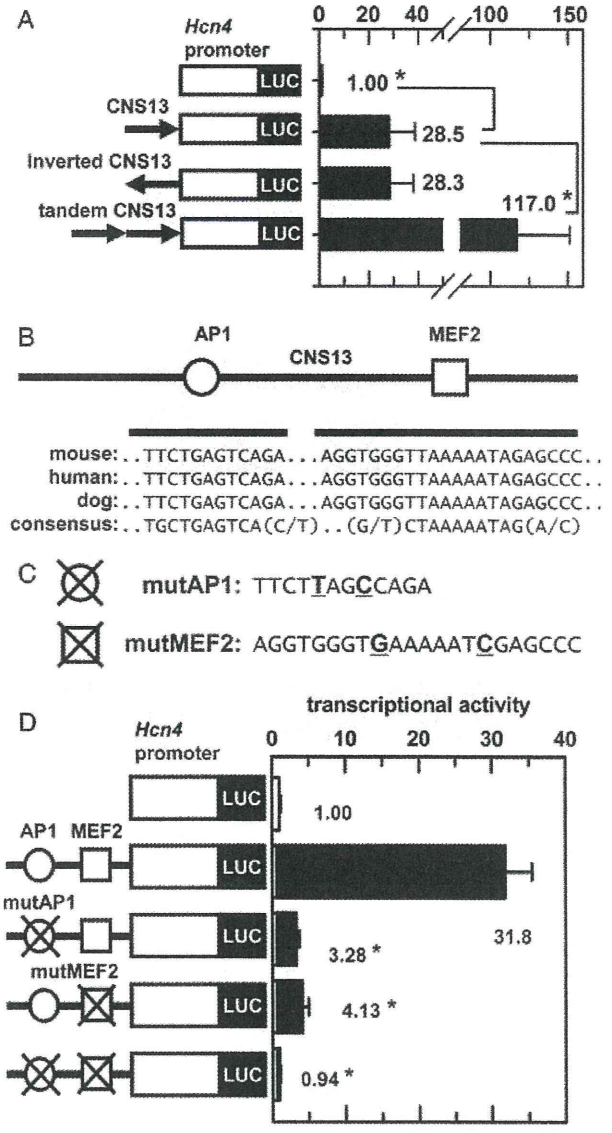

Figure 2 MEF2 and AP1 sites are essential in CNS13. (*A*) A schematic diagram of control, inverted, and tandem CNS13 constructs. The inverted construct was made by swapping the restriction sites at the ends of the control CNS13 fragment. The tandem construct, by introducing *Eco*RI site between the fragments. *$P < 0.05$ compared with control CNS13 construct. (*B*) A schematic diagram of the putative binding sequences for AP1 (open circle) and MEF2 (open square) in CNS13. The AP1 and MEF2 sequences in mouse, human, and dog are aligned with the consensus sequences. The score for the matches were AP1: core match 1.000; matrix match 0.923. MEF2: core match 1.000; matrix match 0.957. (*C*) Mutation of the AP1 and MEF2 sites. The bold, underlined characters indicate the substituted nucleotides. (*D*) Enhancer activity of the CNS13 mutants. Data is presented as relative values to the activity of the *Hcn4* promoter. *$P < 0.05$ compared with *Hcn4* promoter.

We next evaluated enhancer activity for each of the CNS regions using the luciferase reporter assay. In order to achieve this, we linked CNS fragments to the *Hcn4* promoter expressing the luciferase reporter gene in the pGL4.10 vector (*Figure 1B*) and analysed enhancer function in cultured primary cardiomyocytes. As shown in *Figure 1C*, nine CNS fragments (CNS1, 2, 3, 4, 6, 8, 11, 13, and 14) significantly enhanced *Hcn4* promoter activity. The CNS13 construct led to an ~33-fold increase in transcriptional activity, in comparison to the remainder of the constructs that resulted in no more than a 3.2-fold increase.

3.2 MEF2 and AP1 sites are required for the enhancer activity of CNS13

To confirm that CNS13 acts as an authentic enhancer, we next constructed inverted CNS13 and tandem repeated CNS13 fragments and fused with the *Hcn4* promoter. As shown in *Figure 2A*, no significant difference was found between the enhancer activities of normal- and inverted-CNS13 fragments. Tandem repeat CNS13 robustly activated the *Hcn4* promoter. We then focused our study on the CNS13 sequence and explored its *cis*-regulatory mechanism and its potential as a novel enhancer for the *Hcn4* promoter.

To characterize functional motifs in the CNS13 sequence, we searched putative transcription factor binding sites using

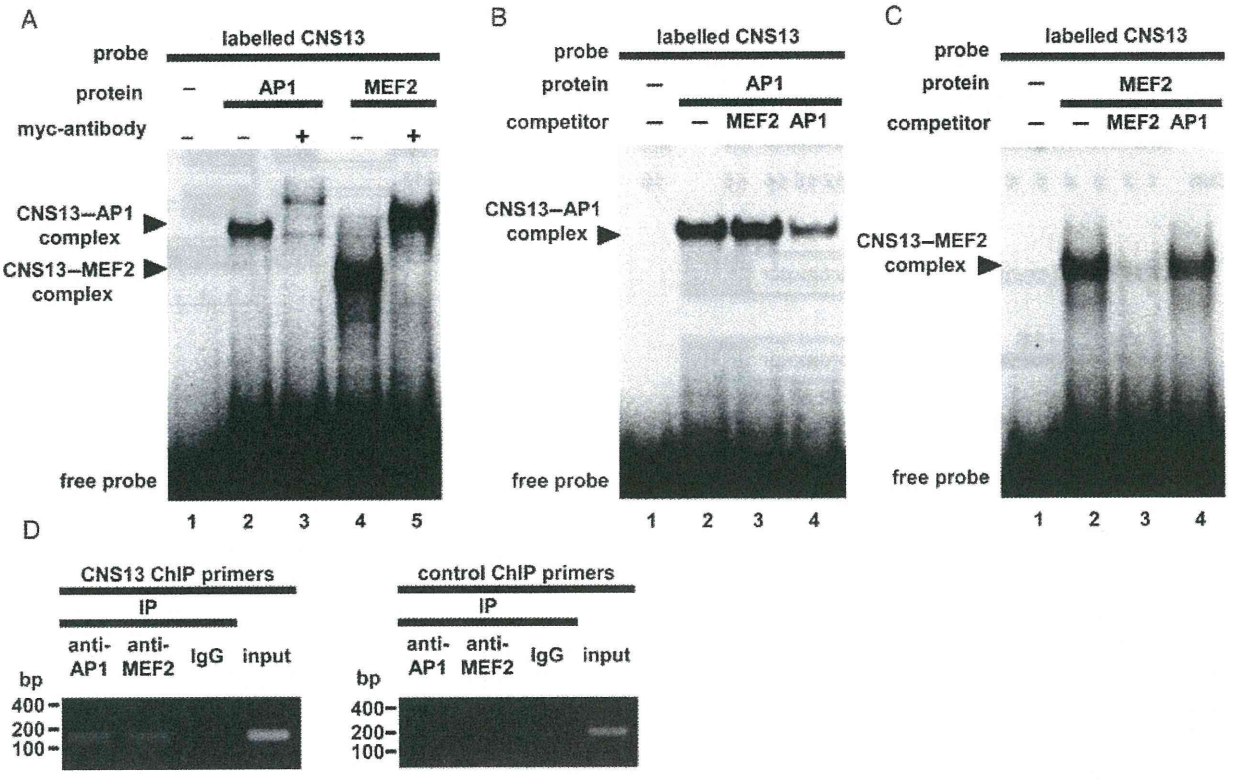

Figure 3 Electrophoretic mobility shift assay (EMSA) and chromatin immunoprecipitation (ChIP) assay using a radiolabelled CNS13 probe. (*A*) EMSA with myc-tagged AP1 and MEF2 proteins. The myc-antibody was used for the supershift assay. (*B*) Competitive EMSAs for the CNS13–AP1 complex. (*C*) CNS13–MEF2 complexes. (*D*) ChIP products using specific antibodies directed against AP1 and MEF2, or a pre-immune IgG were analysed by PCR. Input lane represents PCR products amplified from sonicated chromatin prior to immunoprecipitation. The 152 bp (left) and 200 bp (right) products correspond to CNS13 and distinct genomic regions, respectively.

the TRANSFAC database and detected MEF2- and AP1-binding motifs. As shown in *Figure 2B*, the putative MEF2- and AP1-binding sequences are perfectly conserved among several mammalian species and closely resemble their consensus sequences. These motifs, however, were not conserved in non-mammalian species. We prepared CNS13 reporter constructs harbouring mutations within the MEF2 and AP1 sites (*Figure 2C*) and examined whether enhancer activity was mediated by these sites. As shown in *Figure 2D*, a single mutation in either MEF2- or AP1-binding sequences significantly reduced transcriptional activity, whereas double mutations completely abolished CNS13-induced enhancement. These findings indicate that the *cis*-enhancer function of the CNS13 fragment is dependent on these binding sequences.

We then examined binding of MEF2 and AP1 protein to CNS13. As demonstrated by the electrophoretic mobility shift assay (EMSA) outlined in *Figure 3A*, a slow-migrating band was visualized as a result of interaction between the CNS13 probe and the myc-tagged AP1 protein (lane 2). Another complex was also formed when myc-tagged MEF2 protein was co-incubated with the CNS13 probe (lane 4). Myc-antibody also formed additional complexes (lanes 3 and 5). To precisely identify the DNA sequences recognized by MEF2 and AP1 proteins, we performed competitive EMSA using unlabelled competitors composed of partial CNS13 sequences. As shown in *Figrue 3B*, the signal for the CNS13–AP1 complex was attenuated by the addition of AP1 competitor (lane 4), but not MEF2 competitor (lane 3), indicating that the complex formation is AP1-sequence specific. In CNS13–MEF2 complex competition assays, the opposite patterns were observed (*Figure 3C*). In addition, we amplified a genomic DNA fragment of CNS13 using ChIP with antibodies directed against AP1 and MEF2 (*Figure 3D*). These findings strongly suggest that MEF2 and AP1 transcription factors bind to CNS13 and play an important physiological role in *Hcn4* transcription.

3.3 dnMEF2 resulted in reduced Hcn4 expression

Among the MEF2 family of transcription factors, *MEF2A*, *C*, and *D* are expressed in cardiomyocytes.[10] Given that AP1 is a ubiquitously expressed transcription factor, we focused our study on the physiological role of MEF2. It has previously been shown that MEF2 proteins form hetero- and homodimers and that overexpression of dnMEF2 inhibit its transcriptional activity.[11] The schematic in *Figure 4A* outlines the structure of dnMEF2. In the current study, we demonstrate that dnMEF2 significantly reduced the transcriptional activity of the luciferase reporter vectors and that the enhancer activity of CNS13 was attenuated to 12% of the control levels. When MEF2 binding motif of CNS13 was disrupted, the overexpression of dnMEF2 did not significantly inhibit the enhancer activity (*Figure 4B*).

In order to examine the physiological role of *MEF2 in vivo*, we next expressed dnMEF2 using the AAV1 vector in cardiomyocytes isolated from the inflow tract of the embryonic rat heart, a site in which the HCN4 channel is highly

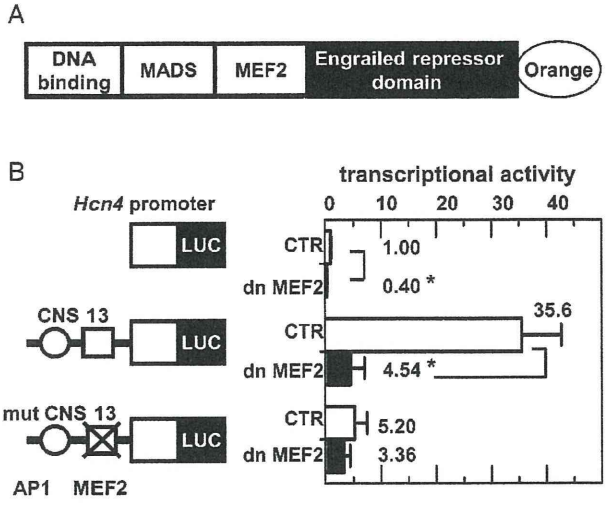

Figure 4 dnMEF2 inhibits *Hcn4* enhancer activity. (*A*) A schematic of the structure of dominant negative MEF2 mutant originated from MEF2C. (*B*) Transcriptional activity of the *Hcn4* promoter and CNS13, but not MEF2 site mutated CNS13, are significantly suppressed by dnMEF2. Along with luciferase reporter constructs, pAAV-dnMEF2 (0.3 μg) or pAAV-GFP (control; 0.3 μg) plasmids were cotransfected. Data are presented as relative values to the activity of the *Hcn4* promoter ($n = 4$; $^*P < 0.05$).

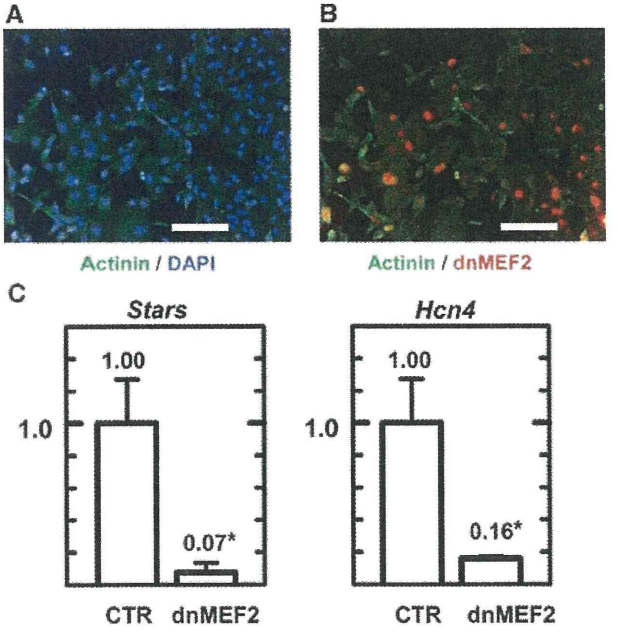

Figure 5 AAV1-dnMEF2 resulted in a reduction in *Stars* and *Hcn4* mRNA levels. (*A*) Immunofluorescent staining of cardiomyocytes for actinin (green). Nucleus is counter stained with DAPI (blue). Approximately 99% of the cells are actinin positive. Bar, 100 μm. (*B*) AAV1-dnMEF2 transfected myocytes demonstrate a nuclear orange fluorescent signal. Approximately 70% of the cells are transfected. (*C*) Relative mRNA levels measured by Q-PCR. Left, *Stars*. Right, *Hcn4*. ($n = 4$; $^*P < 0.05$ vs. control).

expressed.[12] As shown in *Figure 5A*, ~70% of cardiomyocytes was successfully transfected with dnMEF2. Three days following the transfection, *Hcn4* expression levels of Hcn4 were evaluated using real-time PCR. We also evaluated the expression levels of striated muscle activator of Rho signalling (*Stars*), which is known as a direct transcriptional target of MEF2.[13] As shown in *Figure 5A* and *B*, we found

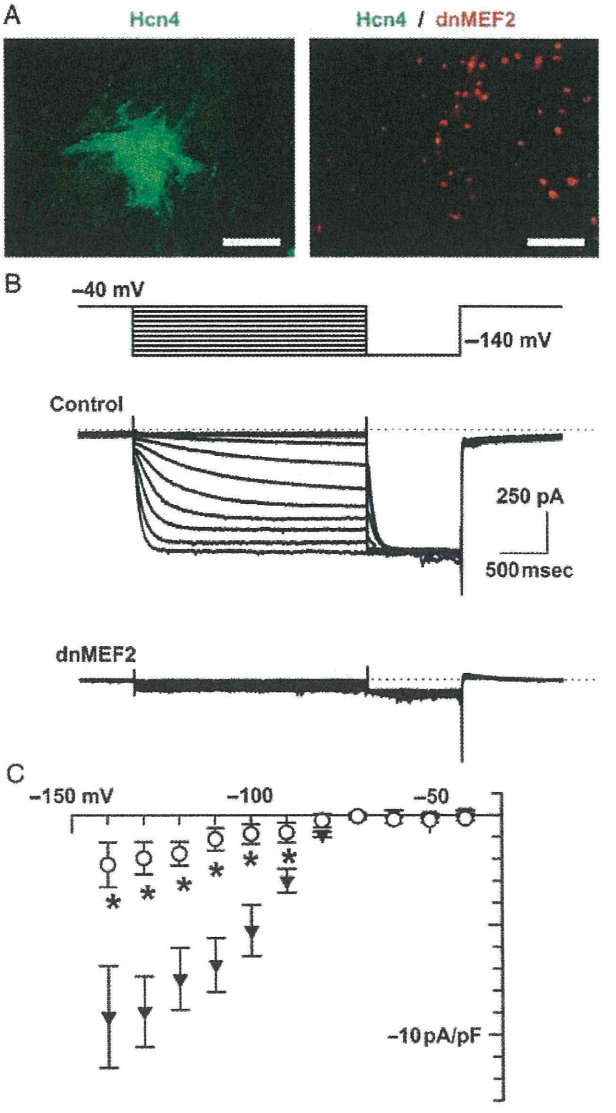

Figure 6 AAV1-dnMEF2 suppressed functional expression of the HCN4 channel. (*A*) Immunostaining for HCN4 (green). Left, control. Right, AAV1-dnMEF2. Bar, 100 μm. (*B*) I_h recorded in embryonic myocytes. The pulse protocol is shown in the top panel. The dotted line indicates the zero current level. (*C*) Current–voltage diagram of I_h. The amplitude of time-dependent current elicited by hyperpolarization was normalized by cellular capacitance. Filled triangle, control; open circle, dnMEF2 ($n = 7$; $^*P < 0.05$).

that both *Stars* and *Hcn4* mRNA levels were significantly reduced in dnMEF2-transfected myocytes, when compared with GFP-transfected myocytes as the negative control. In dnMEF2-transfected myocytes, however, the mRNA levels of HCN1 and HCN2, other types of HCN channels expressed in the heart, were not changed significantly (Supplementary material online, *Figure S1*). These channels might be regulated by different transcriptional mechanisms.[14]

We finally examined the functional expression of the HCN4 channel in embryonic myocytes transfected with dnMEF2. As shown in *Figure 6A* (left panel), HCN4 protein was clearly identified in control myocytes. However, only faint staining of HCN4 protein was observed in the myocytes transfected with dnMEF2 (nuclear-localized orange signals). In accordance with this, robust I_h current was also recorded in the control myocytes (*Figure 6B*, upper traces), whereas I_h